



UvA-DARE (Digital Academic Repository)

S,O-ligand-promoted palladium-catalyzed C–H functionalization of anisole and aniline derivatives

Sukowski, V.

Publication date
2024

[Link to publication](#)

Citation for published version (APA):

Sukowski, V. (2024). *S,O-ligand-promoted palladium-catalyzed C–H functionalization of anisole and aniline derivatives*. [Thesis, fully internal, Universiteit van Amsterdam].

General rights

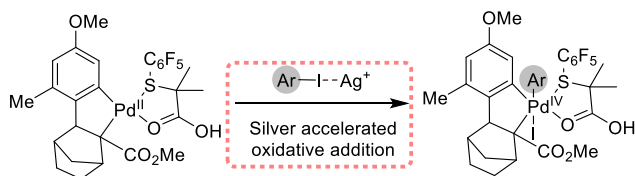
It is not permitted to download or to forward/distribute the text or part of it without the consent of the author(s) and/or copyright holder(s), other than for strictly personal, individual use, unless the work is under an open content license (like Creative Commons).

Disclaimer/Complaints regulations

If you believe that digital publication of certain material infringes any of your rights or (privacy) interests, please let the Library know, stating your reasons. In case of a legitimate complaint, the Library will make the material inaccessible and/or remove it from the website. Please Ask the Library: <https://uba.uva.nl/en/contact>, or a letter to: Library of the University of Amsterdam, Secretariat, P.O. Box 19185, 1000 GD Amsterdam, The Netherlands. You will be contacted as soon as possible.

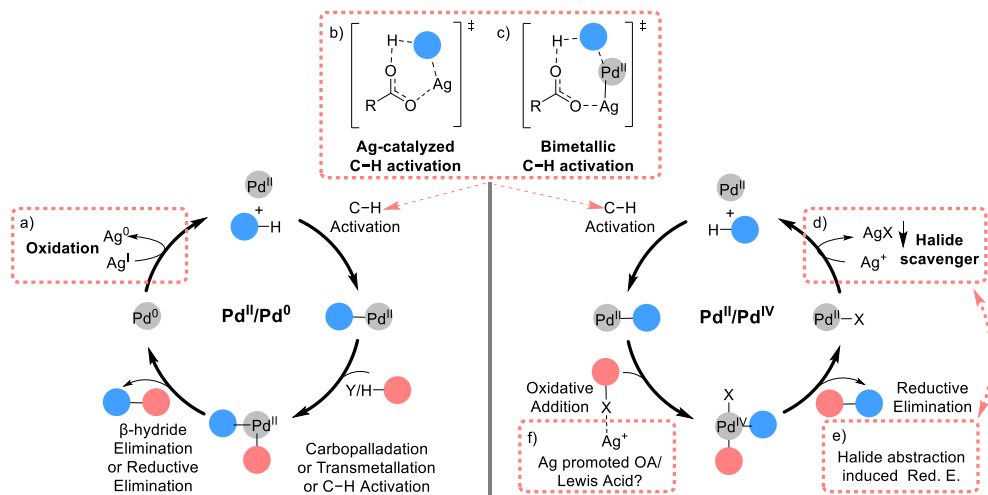
Chapter 6

Mechanistic Insights into the Role of Silver Salts in C–H Arylation Processes Mediated by Palladium/Norbornene Catalysis



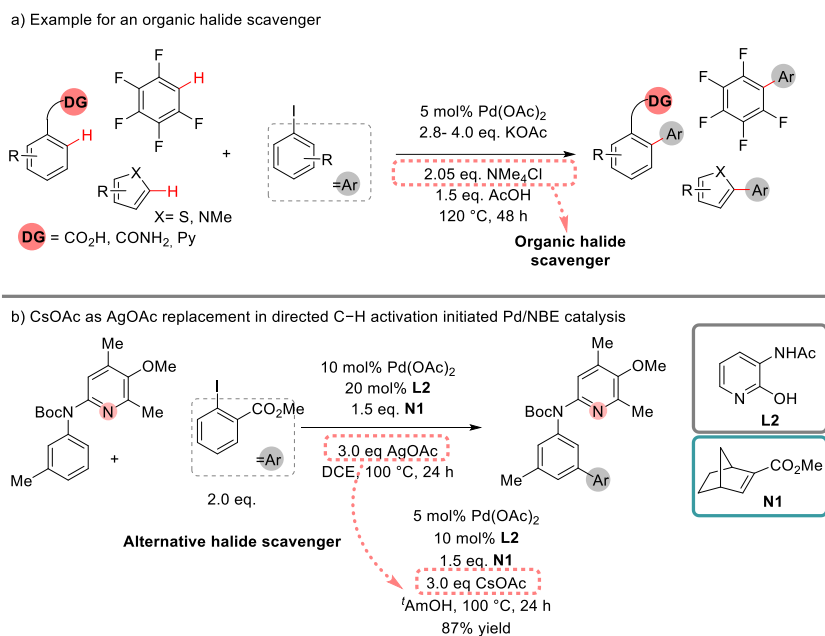
6.1 Introduction

In recent years, Pd-catalyzed C–H functionalization reactions have proven to be an invaluable tool for the synthesis of complex molecules. These reactions offer advantages over traditional cross-coupling reactions due to improved step and atom economy, as no pre-functionalized substrates are required.^[1] However, the frequent use of stoichiometric amounts of silver salts as an additive in many of these methodologies compromises the sustainability aspect of these processes.^[2] Several roles have been attributed to the use of silver salts in C–H functionalization reactions. When a Pd^{II}/Pd⁰ manifold is taking place, i.e. in C–H olefination reactions, silver salt is reported as a terminal oxidant (Scheme 1a).^[2f,3] Recent studies have shown that silver can also be the active catalyst in the C–H activation step^[4] (Scheme 1b) or a co-catalyst forming bi- or multimetallic Pd–Ag complexes (Scheme 1c).^[5] On the other hand, when organic halides are used as reagents, the presence of silver salts is almost ubiquitous. In these processes, which are proposed to operate via the Pd^{II}/Pd^{IV} manifold, silver acts as a halide scavenger to regenerate the active catalyst (Scheme 1d).^[2f, 6–8] Here, it has been assumed that halide abstraction occurs as the last step of the catalytic cycle. However, recent computational studies indicate that in certain cases, halide abstraction occurs prior to the reductive elimination to promote this step (Scheme 1e).^[5g,9,19] In addition to its role as halide scavenger, some authors have suggested that silver may accelerate the oxidative addition of the aryl iodide by acting as a Lewis acid (Scheme 1f).^[2f,10] While this role of silver in palladium catalysis has not been demonstrated experimentally, the group of Ackermann found, using DFT calculations, a lower transition state for the oxidative addition in the presence of silver by acting as a Lewis acid.^[11]



Scheme 1. Possible roles of silver in Pd-catalyzed C–H functionalization. ● = arene substrate ● = introduced FG, X = halide **Roles of Silver**.

If silver is used as the terminal oxidant, it can be replaced by oxygen, organic oxidants,^[12] electrochemical oxidation,^[2f,13] and photoinduced oxidation.^[2f,14] However, finding suitable alternatives to AgOAc when working with organic halides has proven to be a more challenging task and only a limited number of methods have been reported to date.^[5h,15] In 2014 the group of Larrosa reported the replacement of Ag salts by an organic halide scavenger (Scheme 2a).^[15h] In 2016, the group of Yu reported two examples of the modified Catellani reaction, in which AgOAc was replaced by the combination of CsOAc with ^tAmOH as solvent (Scheme 2b).^[15i]



Scheme 2. Examples of additives as substitutes for silver.^[15h,15i]

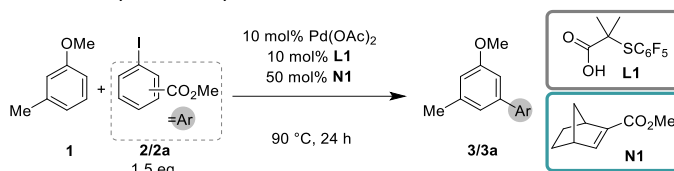
The challenging replacement of silver salts when organic halides are used as reagents led us to consider whether silver plays an additional role that hinders its replacement. In this context, a better understanding of the precise role of silver in these transformations is crucial for the development of silver-free methods. During our investigation of the *meta*-arylation of aryl ethers using Pd/S,O-ligand/NBE catalysis, we successfully isolated several catalytically active Pd-intermediates (Chapter 3). This encouraged us to further explore the role of silver in these transformations.^[16]

In this Chapter, we carry out various kinetic studies on the catalytic and stoichiometric reactions and the isolated palladium-complexes. The experiments were conducted with and without silver and in both HFIP and DCE as the solvent. For the first time, we provide experimental evidence that Ag, in addition to being a halogen scavenger, plays a key role in

promoting the oxidative addition step in palladium catalysis. Notably, we observe that when DCE is used instead of HFIP as a solvent, the use of silver salts is not critical to the reaction, suggesting that the energy barrier for the oxidative addition is lower than with HFIP. Considering the wide range of methodologies involving palladium-catalyzed C–H activation using aryl halides and HFIP as a solvent in the presence of silver additives, we expect our findings to be highly relevant to future investigations towards silver-free C–H functionalization processes.

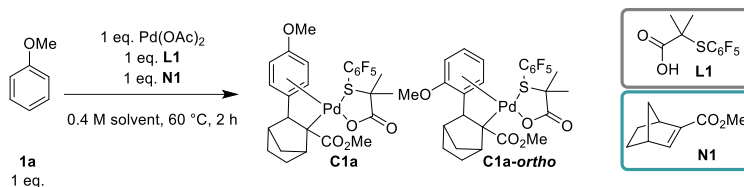
6.2 Results and discussion

Initially, we studied the effect of silver acetate in our *meta*-C–H arylation methodology using 3-methyl anisole (**1**) and methyl 4-iodobenzoate (**2**) as model substrates, 10 mol% of Pd(OAc)₂ and ligand **L1**, and 50 mol% of norbornene **N1**. First, the reaction without silver and with 1.5 eq. of AgOAc were performed using HFIP as solvent. While the reaction in the presence of AgOAc gave a quantitative yield, no product was observed in the absence of silver. This result was unexpected as the reaction should provide a yield of around 10-20% if silver acts only as a halogen scavenger. On the other hand, when DCE and 1.5 eq. of AgOAc were used a moderate yield of 52% was achieved. However, without the addition of AgOAc a 9% yield was obtained, indicating that the reaction occurs without silver, and that silver is acting as halide scavenger to regenerate the active catalyst. Additionally, we tested the reaction using the more reactive aryl iodide **2a**, which facilitates the oxidative addition step,^[2f,10] without AgOAc in both solvents (Table 1, entries 3 and 6). Interestingly, the reaction in HFIP provided the desired product in 6% yield, whereas no product was formed using the less reactive aryl iodide **2**. In DCE, a yield of 16% was obtained. These results suggest that the oxidative addition may be the rate-determining step in HFIP, as the reaction proceeds without silver only when the more reactive aryl iodide **2a** is used.

Table 1. Catalytic *meta*-C–H arylation of aryl ethers.

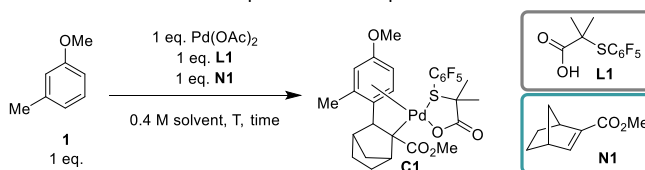
#	Solvent 0.4 M	Aryl-I	Silver salt	¹ H-NMR yield [%] 3
1	HFIP		1.5 eq. AgOAc	100
2	HFIP		-	0
3	HFIP		-	6
4	DCE		1.5 eq. AgOAc	52
5	DCE		-	9
6	DCE		-	16

In our previous work (see Chapter 3),^[16] we were able to isolate the complex resulting from the initial C–H activation and NBE insertion of the unsubstituted anisole (Table 2). Here, the synthesis of the complex was performed using stoichiometric amounts of catalyst and norbornene **N1** in HFIP and DCE. While complete conversion to the **C1a** complexes was observed in HFIP at 60 °C after 2 h, the reaction was apparently slower in DCE (assuming that yield is a reflection of reaction rate) and only 18% yield was achieved (Table 2, entries 1 and 3). In addition, the reaction at rt in HFIP yielded complex **C1a** in 35% and in DCE no complex formation was detected (Table 2, entries 2 and 4). We hypothesized that the higher conversion observed with HFIP is a consequence of the acceleration of the C–H activation step, in line with previous reports where the use of HFIP is key to promoting this step.^[17] Since the formation of these complexes occurs without the addition of silver salts, we propose that silver is not involved in the C–H activation step.^[18]

Table 2. Formation of complex **C1a**.

#	Solvent 0.4 M	Temp. [°C]	Time [h]	¹ H-NMR yield [%] C1a	ratio C1a:C1a-ortho
1	HFIP	60	2	99	1:1.5
2	HFIP	rt	2	35	1:1.7
3	DCE	60	2	18	1:0
4	DCE	rt	2	n.P.	-

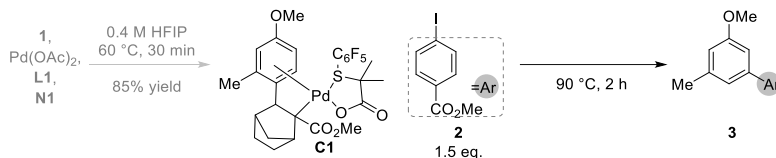
In Chapter 3, we demonstrated by deuterium labeling experiments that the second C–H activation is reversible and occurs at 90 °C in the absence of silver salts, indicating that this step is not rate-limiting and that silver is not involved in this step either. To investigate the following steps after the second C–H activation, we synthesized complex **C1** using 3-methyl anisole (**1**) as this substrate gives only the mono-arylated product under the catalytic conditions, which simplified the interpretation of results. The synthesis of complex **C1** was conducted using stoichiometric amounts of catalyst and norbornene **N1** in HFIP at different temperatures and reaction times (Table 3). We observed at both 90 °C and 60 °C that the NMR yield of **C1** decreased with longer reaction times probably due to its instability. The best yield was obtained at 60 °C stirring the reaction for 0.5 h, providing **C1** in 85% yield.

Table 3. Optimization of reaction time and temperature of complex **C1**.

#	Solvent 0.4 M	Temp. [°C]	Time [h]	¹ H-NMR yield [%] C1
1	HFIP	90	2	70
2	HFIP	90	4	40
3	HFIP	60	0.25	76
4	HFIP	60	0.5	85
5	HFIP	60	1	70
6	HFIP	60	2	70

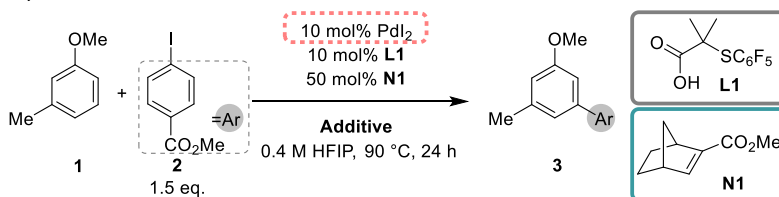
Next, we studied the reactivity of complex **C1** with aryl iodide **2**, with and without AgOAc in HFIP and DCE (Table 4). Due to the instability of **C1** during purification, the crude reaction was used after a simple filtration through celite and concentration under reduced pressure. The reaction performed in HFIP with AgOAc provided 75% of the arylated product **3**, while only 10% yield of **3** was obtained in the absence of AgOAc (Table 4, entries 1-2). In the latter, only 41% of complex **C1** was observed in the crude mixture, probably due to the decomposition of the complex over time. A completely different scenario was observed when DCE was used as a solvent. In both cases with and without silver, 70% and 61% yield of the arylated product was achieved (Table 4, entries 3-4). These results indicate that silver acts exclusively as a halogen scavenger when DCE is used as solvent as the intermediate palladium complex **C1** as well as the final arylated product **3** are obtained in the absence of silver salts. On the other hand, we observed that silver has a strong influence on the reactivity of the complex **C1** with the aryl iodide **2** in HFIP, indicating its additional role in potentially promoting the oxidative addition step.

Table 4. Arylation reaction with complex **C1**.



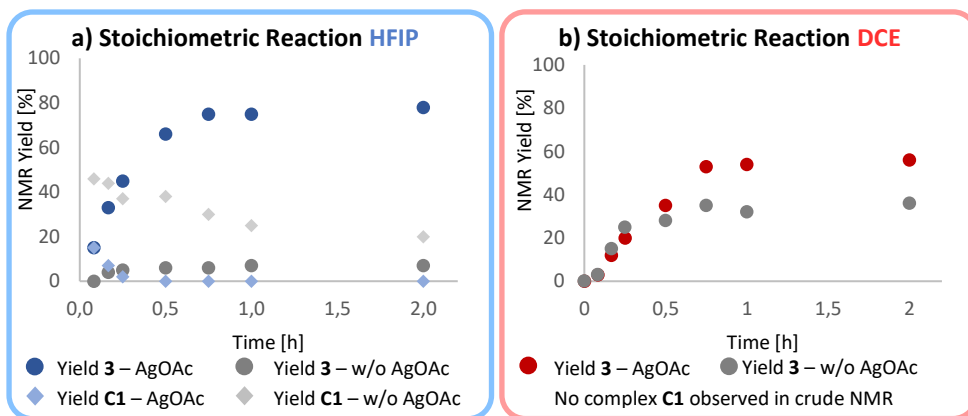
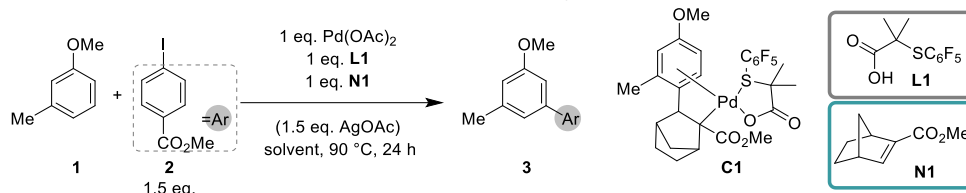
#	Solvent 0.4 M	Silver Salt	¹ H-NMR yield [%] 3	¹ H-NMR yield [%] C1
1	HFIP	1.5 eq. AgOAc	75	-
2	HFIP	-	10	41
3	DCE	1.5 eq. AgOAc	70	-
4	DCE	-	61	10

It is important to note that regardless of the solvent chosen, AgOAc is likely to act as a halide scavenger for the regeneration of the active catalyst.^[19] To provide further support for this hypothesis, the catalytic reaction was carried out using PdI_2 as the precatalyst with various additives (Table 5). As expected, only the reactions with AgOAc gave the desired arylated product in both HFIP and DCE. In contrast, reactions without any additive or with KOAc did not result in any observable product formation, regardless of the solvent used. It can then be concluded that AgOAc acts as a halogen scavenger for catalyst regeneration in both solvents.

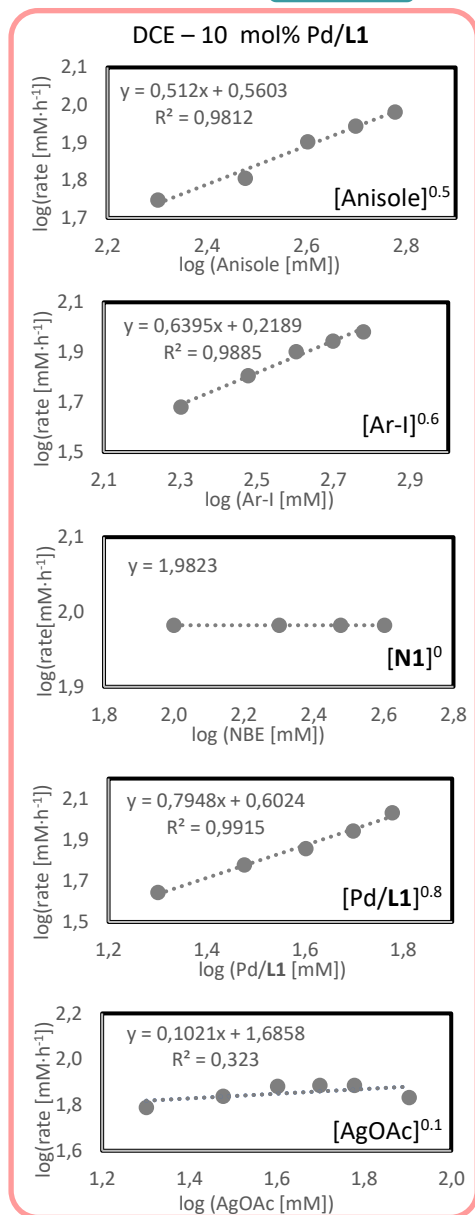
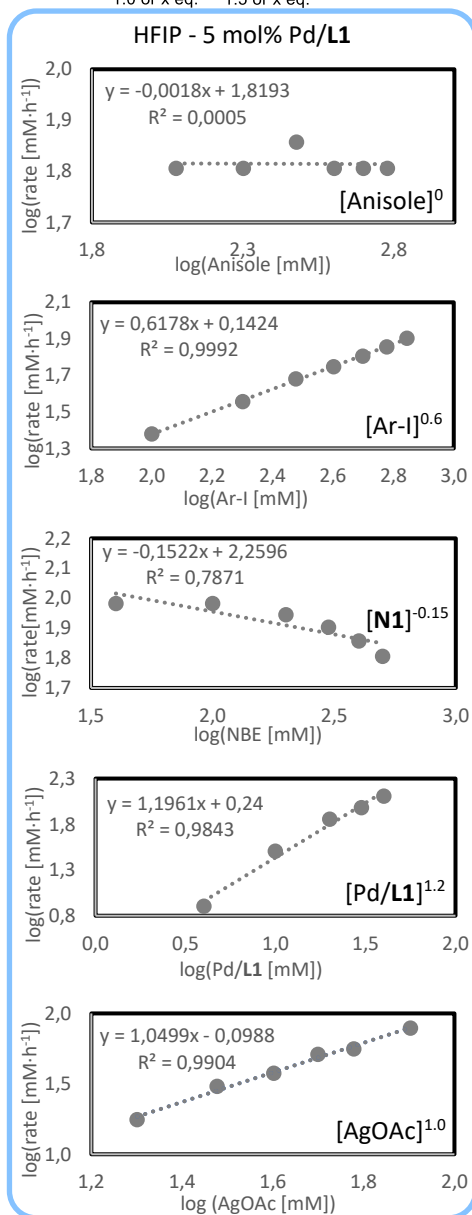
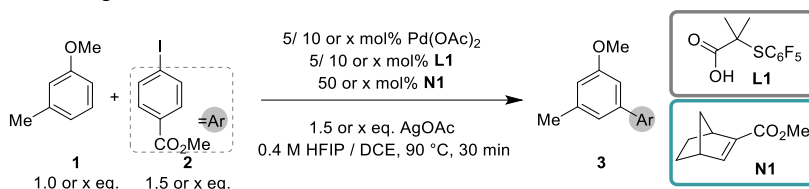
Table 5. Catalytic reaction with PdI₂ with different additives.

#	Solvent 0.4 M	Additive	¹ H-NMR yield [%] 3
1	HFIP	1.5 eq. AgOAc	90
2	HFIP	1.5 eq. KOAc	n.P.
3	HFIP	-	n.P.
4	DCE	1.5 eq. AgOAc	42
5	DCE	1.5 eq. KOAc	n.P.
6	DCE	-	n.P.

To gain further insight into the role of silver in the reaction, we carried out kinetic studies using stoichiometric amounts of catalyst in both HFIP and DCE with and without AgOAc (Table 6). For the reaction in HFIP, 80% yield was achieved after 45 min in the presence of 1.5 eq. AgOAc and without AgOAc, a low yield of up to 8% was observed even after several hours. Interestingly, in the reaction without silver, complex **C1** was the main product in solution, and its concentration decreased with time as the concentration of the starting anisole increased (see Experimental section). This result indicates that the oxidative addition does not occur efficiently in the absence of silver salts. When the reaction was performed in the presence of AgOAc, 15% of the desired product **3** and 15% of complex **C1** was observed after 8 min, the latter almost disappeared after 25 min of reaction, and **3** was obtained in 82% yield after 15 h. These results can be interpreted by an accumulation of complex **C1** in an initial or inductive period, which is then consumed (Table 6a). A completely different scenario was observed when the reaction was carried out in DCE. The initial rate of the reaction was identical up to approximately 30 min of reaction time. Only after this point, the reaction without AgOAc exhibited a lower conversion. These results indicate that silver has no effect on the oxidative addition step in DCE. The higher conversion observed after 30 min of reaction with AgOAc can be attributed to the reoxidation of Pd⁰ to Pd^{II}, as Pd^{II} is reduced *in situ* during the reaction (Table 6b). In addition, the reaction in the presence of AgOAc is faster in HFIP than in DCE, which can be attributed to the enhanced reaction rate of the C–H activation step in HFIP (*vide supra*). The lower yield of the arylated product **3** in DCE can be explained by the deactivation of the palladium catalyst as a consequence of the overall lower reaction rate.

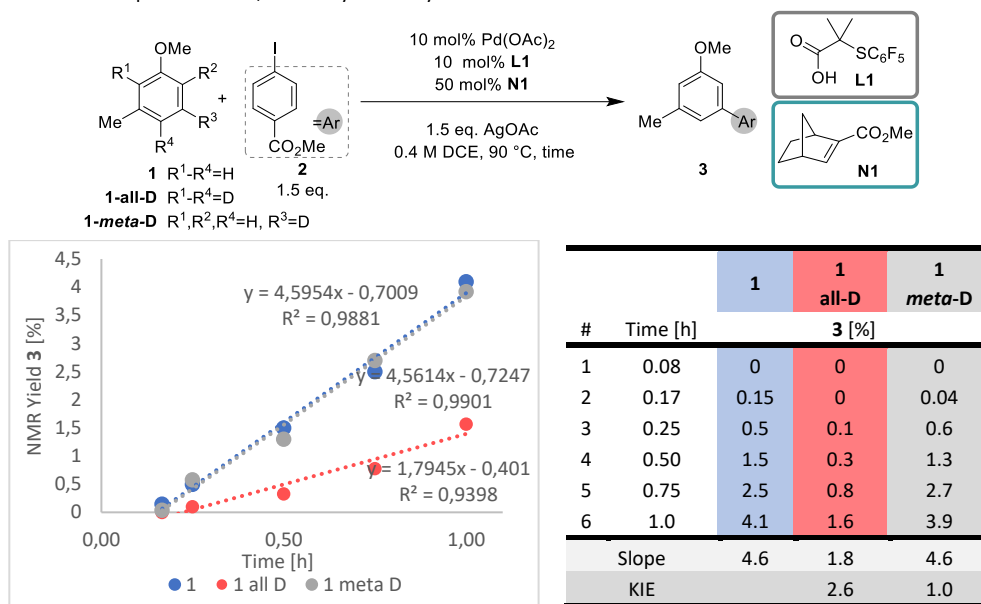
Table 6. Kinetic profile of stoichiometric reaction with and without AgOAc in HFIP and DCE.

To provide further evidence for the role of silver in accelerating the oxidative addition step in the catalytic reaction, we performed initial rate kinetics to determine the kinetic order of each reagent in HFIP and DCE (Table 7). In HFIP an order of zero was determined for anisole derivative **1**, confirming that the C–H activation is not the rate determining step. An order of 0.6 for Ar-I, -0.15 for NBE, 1.2 for the catalyst and 1.0 for AgOAc were obtained. These results indicate that the oxidative addition is rate limiting and silver is involved in this step. We explained the 0.6 order of Ar-I, and not 1 as it should be, by off-cycle reactions such as those involved in the formation of the side product **SP1** (see Chapter 3). Norbornene shows a saturation curve leading to an overall order of -0.15. This is the first experimental evidence that silver salts can be involved in promoting the oxidative addition step. In DCE, anisole derivative **1** and Ar-I exhibited a kinetic order of 0.5 and 0.6, respectively. The kinetic order of catalyst is 0.8 and zero for norbornene. Interestingly, the kinetic order of AgOAc was close to zero, indicating its negligible involvement in either the C–H activation or oxidative addition step. To explain these results, we speculate that the activation energy for both C–H activation and oxidative addition are similar in DCE.

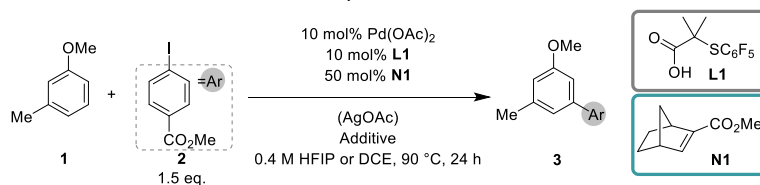
Table 7. Order of reagents via initial rate kinetics in HFIP and DCE.

Next, we measured the KIE for both the first and the second C–H activation in DCE by performing the reactions with 1-methoxy-3-methylbenzene **1**, substrate 1-methoxy-3-methylbenzene-2,4,5,6-*d*₄ (**1-all-D**) and substrate 1-methoxy-3-methylbenzene-5-*d*₄ (**1-meta-D**) in separate flasks (Table 8). The K_H/K_D ratio was determined to be 2.6 for **1-all-D** and 1.0 for **1-meta-D**. The observed primary KIE for **1-all-D**, suggests that either the first or the second C–H activation is involved in the rate-determining step. However, as a KIE of 1.0 was measured for **1-meta-D**, we conclude that the first C–H activation is involved in the rate-determining step. Further studies are needed to confirm that the activation energy for both C–H activation and oxidative addition are similar in DCE.

Table 8. KIE experiment of *N,N*-dibenzyl-3-methylaniline **1b**.



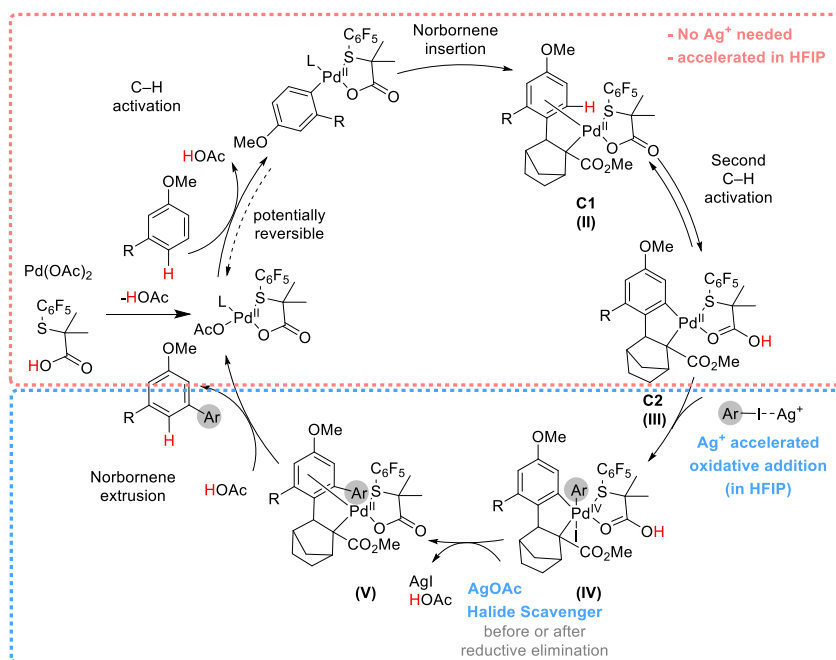
Finally, we decided to investigate the possibility of replacing silver salts in the reaction. Under the optimal conditions, we investigated various additives as potential replacements for AgOAc (Table 9). Considering the distinct roles of AgOAc in HFIP and DCE, both solvents were examined in our study. In HFIP, we observed that reducing the amount of AgOAc to 0.5 eq. resulted in a yield reduction of 40%. The impact of bases like KOAc^[2f] or NMe₄OAc^[15h], which could potentially serve as halide scavengers, was also explored. To determine whether these additives have a negative effect on reactivity and whether only a small amount of silver is required to promote the oxidative addition step and whether the additives can act as halogen scavengers, the reactions were first carried out with 1.5 and 0.5 eq. of AgOAc (Table 9, entries 4-7). We found in both cases that neither KOAc nor NMe₄OAc affected the reactivity. Subsequently, we explored various additives, but we found that without the presence of a Ag salt, no yield was obtained (Table 9, entries 8-13). On the other hand, when DCE is used as a solvent, silver is only responsible for the catalyst regeneration. The effect of different acetate bases was explored. The addition of a potassium base as well as NMe₄OAc^[15h] completely inhibited the reaction, even when AgOAc (Table 9, entries 16-18) or 5 eq. of HFIP (Table 9, entry 19) were added. Only Mg(OAc)₂, Ca(OAc)₂ and Ba(OAc)₂ gave yields of around 6-11% (Table 9, entries 22-24), indicating that the reaction was not inhibited, but rather hindered by lack of catalyst regeneration. So far we have not been able to find any other reagent or combination of reagents to replace the silver salt. However, we are confident that a better understanding of the role of silver in different solvents will aid future attempts.

Table 9. Evaluation of different additives in *meta*-arylation of anisole **3**.

#	Solvent 0.4 M	Silver Salt	Additive	¹ H-NMR yield [%] 3
1	HFIP	1.5 eq. AgOAc	-	100
2	HFIP	0.5 eq. AgOAc	-	40
3	HFIP	-	-	n.P.
4	HFIP	1.5 eq. AgOAc	1 eq. KOAc	95
5	HFIP	0.5 eq. AgOAc	1 eq. KOAc	39
6	HFIP	1.5 eq. AgOAc	1 eq. NMe ₄ OAc	90
7	HFIP	0.5 eq. AgOAc	1 eq. NMe ₄ OAc	39
8	HFIP	-	1.5 eq. KOAc	n.P.
9	HFIP	-	1.5 CsOAc	3
10	HFIP	-	1.5 eq. Mg(OAc) ₂ • 4 H ₂ O	n.P.
11	HFIP	-	1.5 eq. Ca(OAc) ₂	n.P.
12	HFIP	-	1.5 eq. Ba(OAc) ₂	n.P.
13	HFIP	-	1.5 eq. ScOTf ₃	n.P.
14	DCE	1.5 eq. AgOAc	-	52
15	DCE	-	-	9
16	DCE	1.5 eq. AgOAc	1 eq. KOAc	traces
17	DCE	1.5 eq. AgOAc	1 eq. NMe ₄ OAc	n.P.
18	DCE	-	1.5 eq. KOAc	n.P.
19	DCE	-	1 eq. KOAc/ 5 eq. HFIP	n.P.
20	DCE	-	0.5 eq. K ₂ CO ₃	4
21	DCE	-	0.5 eq. NMe ₄ OAc	n.P.
22	DCE	-	1.5 eq. Mg(OAc) ₂ • 4 H ₂ O	6
23	DCE	-	1.5 eq. Ca(OAc) ₂	9
24	DCE	-	1.5 eq. Ba(OAc) ₂	11

6.3 Conclusion

In summary, we have performed various kinetic studies with and without silver to elucidate its role in the *S,O*-ligand promoted non-directed *meta*-arylation in Pd/NBE catalysis. We have proven that HFIP promotes the C–H activation steps and that AgOAc is not involved in these steps. Experimentally, we have observed that the oxidative addition is the rate-determining step in HFIP and that silver is required to promote this step. This is the first experimental evidence that Ag, in addition to being a halogen scavenger, plays a key role in promoting the oxidative addition step in palladium catalysis. Notably, we have observed in the stoichiometric reaction that when DCE was used as solvent instead of HFIP, the presence of silver salts was not critical for the reaction, suggesting that the energy barrier for the oxidative addition is lower than with HFIP. Considering the wide range of methodologies involving palladium-catalyzed C–H activation using aryl halides in HFIP with silver additives, we expect our finding to be highly relevant for future investigations towards silver-free C–H functionalization processes.



Overview: Role of silver in the catalytic reaction.

6.4 Experimental section

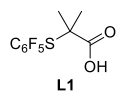
General information

Chromatography: Flash column chromatography was performed using Macherey-Nagel Silica 60 (particle size 0.04–0.063 mm) under compressed air flow or a Buchi C-850 automatic column machine with FlashPure silica cartridges, TLC: Merck TLC plates (0.25 mm) precoated with silica gel 60 F₂₅₄. Visualization of the TLC was performed by UV and KMnO₄. High-resolution mass spectra (HRMS) were recorded on an AccuTOF GC v 4g, JMST100GCV mass spectrometer (JEOL, Japan) and HR-ToF Bruker Daltonik GmbH (Bremen, Germany) Impact II, an ESI-ToF MS capable of resolution of at least 40,000 FWHM. The FD/FI probe was equipped with an FD Emitter, Carbotec, FD = 10 μm. Current rate = 51.2 mA/min over 1.2 min using field desorption (FD) as an ionization method. Bruker DRX-300, 400 and 500 MHz instruments were used to record NMR spectra. Chemical shift values are reported in ppm with the solvent resonance as the internal standard (CDCl₃: δ 7.26 for ¹H, δ 77.16 for ¹³C). Data are reported as follows: chemical shifts, multiplicity (s = singlet, d = doublet, dd = doublet of doublets, t = triplet, dt = doublet triplet, bs = broad singlet, m = multiplet), coupling constants (Hz), and integration. ATR technique was used in IR spectroscopy on a Bruker Alpha-P. Melting points (M.P.) were measured in Buchi M-565 melting point apparatus. All reagents and solvents were used as received. Pd(OAc)₂ was purchased from Strem.

Characterization of reagents

The synthesis and full characterization of the ligand **L1**, NBE **N1** and Product **3** can be found in literature.^[16]

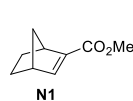
2-Methyl-2-[(perfluorophenyl)thio]propanoic acid (**L1**)



White solid, ¹H NMR (400 MHz, CDCl₃) δ 1.56 (s, 6H). ¹⁹F NMR (376 MHz, CDCl₃) δ -128.46 – -129.66 (m), -147.81 – -149.16 (m), -160.15 – -161.52 (m). ¹³C NMR (101 MHz, CDCl₃) δ 178.71, 150.71 – 149.63 (m), 148.52 – 147.16 (m), 144.69 – 143.69 (m), 141.90 – 141.27 (m), 139.19 – 138.48 (m), 136.65 – 135.97 (m), 51.72, 24.82. ¹H NMR of the isolated material matched with that reported in

the literature.^[16]

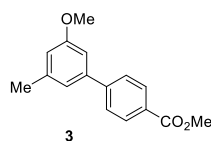
Methylbicyclo[2.2.1]hept-2-ene-2-carboxylate (**N1**)



Clear oil, R_f = 0.24 (Cy / DCM = 1:1). ¹H NMR (400 MHz, CDCl₃) δ 6.92 (d, J = 3.3 Hz, 1H), 3.72 (s, 3H), 3.25 (s, 1H), 3.01 (dq, J = 3.3, 1.6 Hz, 1H), 1.93 – 1.63 (m, 2H), 1.48 (dp, J = 8.4, 2.1 Hz, 1H), 1.20 (dq, J = 8.5, 1.3 Hz, 1H), 1.08 (dddd, J = 13.0, 9.0, 6.6, 2.2 Hz, 2H). ¹³C NMR (101 MHz, CDCl₃) δ 165.49, 147.16, 140.85, 51.42, 48.34, 43.63, 42.05, 24.74, 24.61. ¹H NMR of the isolated

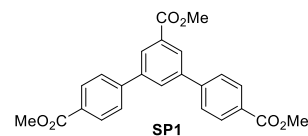
material matched with that reported in the literature.^[16]

Methyl 3'-methoxy-5'-methyl-[1,1'-biphenyl]-4-carboxylate (**3**)

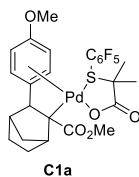


White solid, R_f = 0.34 (Cy / DCM = 1:1). ¹H NMR (400 MHz, CDCl₃) δ 8.09 (d, J = 8.2 Hz, 2H), 7.64 (d, J = 8.2 Hz, 2H), 7.03 (s, 1H), 6.96 (s, 1H), 6.77 (s, 1H), 3.94 (s, 3H), 3.86 (s, 3H), 2.41 (s, 3H). ¹³C NMR (101 MHz, CDCl₃) δ 167.08, 160.16, 145.78, 141.39, 139.83, 130.11, 129.03, 127.18, 120.77, 114.48, 110.20, 55.41, 52.20, 21.76. ¹H NMR of the isolated material matched with that reported in the literature.^[16]

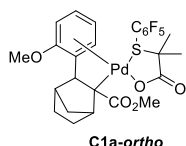
Trimethyl [1,1':3',1''-terphenyl]-4,4'',5'-tricarboxylate (**SP1**)



Generally, the side-product was observed, if the aryl ether substrate showed a low reactivity. White solid, ¹H NMR (400 MHz, CDCl₃) δ 8.32 (d, J = 1.8 Hz, 2H), 8.16 (d, J = 8.5 Hz, 4H), 8.03 (t, J = 1.8 Hz, 1H), 7.75 (d, J = 8.5 Hz, 4H), 4.00 (s, 3H), 3.96 (s, 6H). ¹³C NMR (101 MHz, CDCl₃) δ 166.95, 166.73, 144.35, 141.32, 131.78, 130.55, 130.44, 129.82, 128.12, 127.38, 52.62, 52.39. HRMS (FD): m/z calculated for C₁₆H₁₆O₃ [M]⁺ = 404.1260; found = 404.1272. IR (neat): ν_{max} (cm⁻¹): 2952, 1720, 1609, 1435, 1344, 1278, 1244, 1190, 1110, 1055, 1018, 854, 762, 749.^[16]

Complex C1a

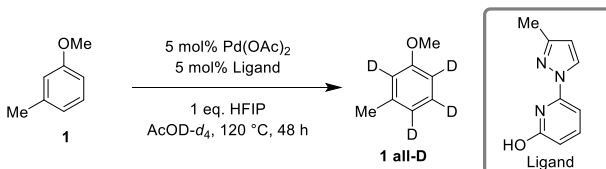
Complex **C1a** was synthesized by adding anisole (165 μL , 1.5 mmol, 1.0 eq), $\text{Pd}(\text{OAc})_2$ (342 mg, 1.5 mmol, 1.0 eq), **N1** (228 mg, 1.5 mmol, 1.0 eq.), **L1** (429 mg, 1.5 mmol, 1.0 eq) and HFIP (3.75 mL, 0.4 M) in a pressure tube and the mixture stirred for 2 h at 90 $^\circ\text{C}$. After cooling to room temperature, the reaction was filtrated through Celite[®] and rinsed with DCM. Purification by column chromatography on silica gel using EtOAc / MeOH(1:0-9:1 v/v) as an eluent provided the title compound as an orange solid (71% yield, 692 mg, 1.07 mmol). $R_f = 0.74$ (EtOAc / MeOH = 50:1). $^1\text{H NMR}$ (400 MHz, CDCl_3) δ 8.16 (d, $J = 7.8$ Hz, 1H), 7.83 (d, $J = 8.6$ Hz, 1H), 7.19 (d, $J = 8.1$ Hz, 1H), 6.99 (d, $J = 7.0$ Hz, 1H), 3.85 (s, 3H), 3.56 (s, 1H), 3.38 (s, 3H), 3.04 (d, $J = 10.1$ Hz, 1H), 2.64 (d, $J = 3.6$ Hz, 1H), 2.21 (s, 1H), 1.68 – 1.57 (m, 2H), 1.48 (s, 3H), 1.39 (ddd, $J = 20.5, 10.5, 4.2$ Hz, 1H), 1.27 (s, 3H), 1.24 – 1.17 (m, 1H), 1.13 – 1.04 (m, 1H). $^1\text{H NMR}$ of the isolated material matched with that reported in the literature.^[16]

Complex C1a-ortho

Representative signals: $^1\text{H NMR}$ (400 MHz, CDCl_3) δ 8.07 (d, $J = 7.2$ Hz, 1H), 7.60 (t, $J = 7.6$ Hz, 1H), 7.17 (t, $J = 7.4$ Hz, 1H), 7.09 (d, $J = 8.3$ Hz, 1H), 4.03 (s, 3), 3.20 – 2.96 (m, 1H), 2.41 – 2.20 (m, 1H), 1.60 (s, 3H), 1.34 (s, 3H). $^{13}\text{C NMR}$ (101 MHz, CDCl_3) δ 179.71, 136.27, 129.53, 122.98, 113.98, 76.07, 60.91, 55.19, 44.50.^[16]

Procedure for the synthesis of 1-methoxy-3-methylbenzene-2,4,5,6-*d*₄ (1 all-D**)**

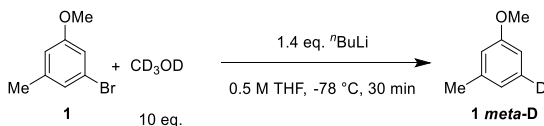
The deuterated 1-methoxy-3-methylbenzene-2,4,5,6-*d*₄ was prepared following the procedure described in the literature.^[20]



In a pressure tube containing a suitable stirring bar, $\text{Pd}(\text{OAc})_2$ (11 mg, 0.05 mmol, 5 mol%), Ligand (9 mg, 0.05 mmol, 5 mol%), 1-methoxy-3-methylbenzene (126.0 μL , 1 mmol, 1.0 eq.), HFIP (105 μL , 1 mmol, 1.0 eq.) $\text{AcOD-}d_4$ (5.0 mL, 0.2 M) were added. The tube was placed into a pre-heated oil bath at 120 $^\circ\text{C}$ and stirred for 48 h. After cooling to room temperature, a 10% NaOH solution was added and the mixture extracted with EtOAc ($\times 3$). The combined organic layers were dried over anhydrous MgSO_4 , filtered and concentrated under reduced pressure. Purification by column chromatography on silica gel using Pentane as an eluent provided the title compound as a clear oil (108.9 mg, 86% yield). $^1\text{H NMR}$ (300 MHz, CDCl_3) δ 3.81 (s, 3H), 2.35 (s, 3H). $^{13}\text{C NMR}$ (101 MHz, CDCl_3) δ 159.63, 139.42, 129.23 – 128.34 (m), 121.52 – 120.79 (m), 114.88 – 114.23 (m), 110.92 – 110.16 (m), 55.23, 21.55 **HRMS** (FI): m/z calculated for $\text{C}_8\text{H}_6\text{D}_4\text{O}$ $[\text{M}]^+ = 126.0983$; found = 126.0988. **IR** (neat): ν_{max} (cm^{-1}): 2957, 1261, 1083, 1068, 1053, 1020, 800, 421.

Procedure for the synthesis of 1-methoxy-3-methylbenzene-5-*d* (1 meta-D**)**

The deuterated 1-methoxy-3-methylbenzene-5-*d* was prepared following the procedure described in the literature.^[21]



1-methoxy-3-methylbenzene (0.73 mL, 5 mmol, 1.0 eq.) was dissolved in anhydrous THF (10 mL, 0.5 M) under nitrogen atmosphere, and the solution was cooled to -78 $^\circ\text{C}$. Then, a solution of $n\text{BuLi}$ (2.8 mL, 7.0 mmol, 1.4 eq.,

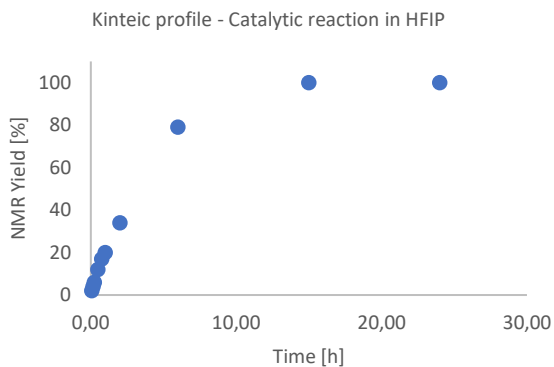
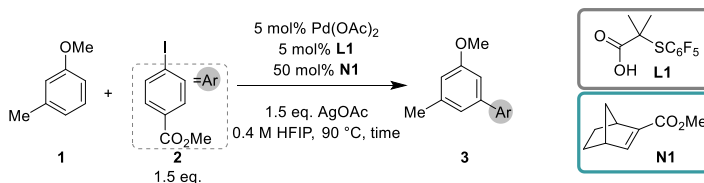
2.5 M in hexanes) was added slowly. The reaction mixture was stirred 30 min. Then the reaction was quenched with CD₃OD (2.0 mL, 50 mmol, 10 eq.) stirred at -78 °C for 30 min. Water was added and the mixture was extracted with Et₂O (× 3). The combined organic layers were dried over anhydrous MgSO₄, filtered and concentrated under reduced pressure. Purification by column chromatography on silica gel using Pentane as an eluent provided the title compound as a clear oil (590 mg, 96% yield). ¹H NMR (300 MHz, CDCl₃) δ 6.77 (s, 1H), 6.75 – 6.66 (m, 2H), 3.80 (s, 3H), 2.34 (s, 3H). ¹³C NMR (101 MHz, CDCl₃) δ 159.71, 139.62, 129.31 – 128.77 (m), 121.51, 114.86, 110.80, 55.25, 21.69. HRMS (FI): *m/z* calculated for C₈H₆D₄O [M]⁺ = 123.0794; found = 123.0794. IR (neat): *v*_{max} (cm⁻¹): 2956, 2929, 1596, 1463, 1152, 421.

Procedure for kinetic isotope effect

18 pressure tube containing a suitable stirring were equipped AgOAc (25.0 mg, 0.15 mmol, 1.5 eq.) and methyl 4-iodobenzoate (40.1 mg, 0.15 mmol, 1.5 eq.). Then, six pressure tubes were charged 1-methoxy-3-methylbenzene **1** (12.8 mg, 0.1 mmol, 1.0 eq.), other six pressure tubes with 1-methoxy-3-methylbenzene-2,4,5,6-*d*₄ **1-all-D** (12.8 mg, 0.1 mmol, 1.0 eq.) and the remaining six pressure tubes with 1-methoxy-3-methylbenzene-5-*d* **1-meta-D** (12.8 mg, 0.1 mmol, 1.0 eq.). After, all 18 pressure tubes were equipped with 100 μL stock solution containing Pd(OAc)₂ (0.01 mmol, 10 mol%, 0.1 M in DCE), ligand **L1** (0.01 mmol, 10 mol%, 0.1 M in DCE), NBE **N1** (0.01 mmol, 10 mol%, 0.1 M in DCE). Then 0.15 mL of DCE (0.4 M) was added. All 18 pressure tubes were placed in a pre-heated oil bath at 90 °C and stirred for the indicated time. The reaction tube was cooled in an ice bath and filtered through Celite® and rinsed with EtOAc. To the crude mixture CH₂Br₂ (7.08 μL, 0.1 mmol) was added as internal standard, the mixture was dissolved in CDCl₃ and ¹H NMR was measured.

Kinetic profile of catalytic reaction – HFIP

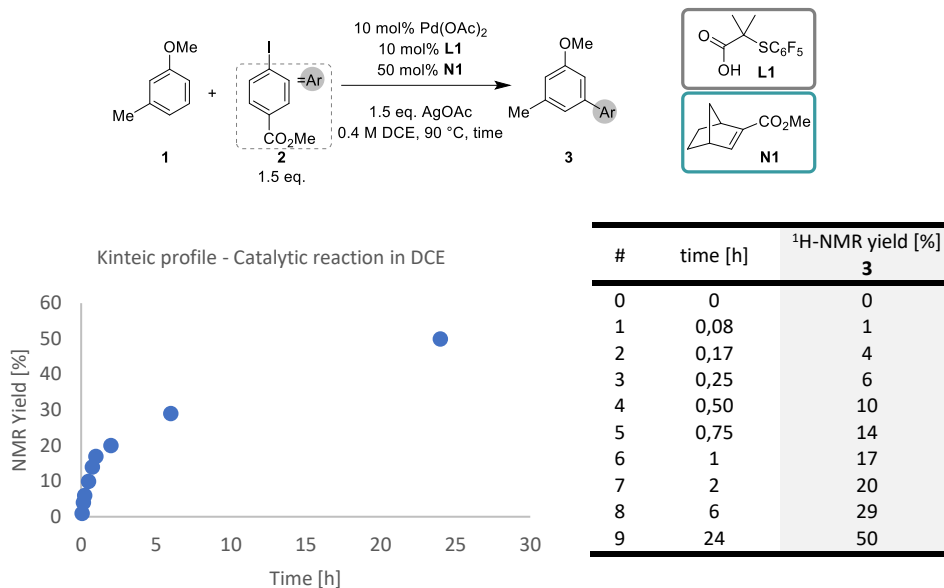
A stock solution of 3-methylanisole **1** (76.4 μL , 0.6 mmol, 1.0 eq.), methyl 4-iodobenzoate (240.6 mg, 0.9 mmol, 1.5 eq.), **N1** (45.6 mg, 0.3 mmol, 0.5 eq.), Pd(OAc)₂ (6.6 mg, 0.03 mmol, 5 mol%), S,O-ligand **L1** (8.6, 0.03 mmol, 5 mol%) in 1.5 mL HFIP was prepared. Ten pressure tubes containing a suitable stirring were equipped with AgOAc (12.5 mg, 0.075 mmol, 1.5 eq.) and 150 μL of the stock solution (reaction scale: 0.05 mmol). The tubes were placed in a pre-heated oil bath at 90 °C and stirred for the indicated time. The reaction tube was cooled in an ice bath and filtered through Celite® and rinsed with DCM. To the crude mixture CH₂Br₂ (3.54 μL , 0.05 mmol) was added as internal standard, the mixture was dissolved in CDCl₃ and ¹H NMR was measured.

Table 10. Kinetic profile of catalytic reaction – HFIP.

#	time [h]	¹ H-NMR yield [%] 3
0	0	0
1	0,08	2
2	0,17	4
3	0,25	6
4	0,50	12
5	0,75	17
6	1	20
7	2	34
8	6	79
9	15	100
10	24	100

Kinetic profile of catalytic reaction - DCE

9 pressure tubes containing a suitable stirring were equipped with 3-methylanisole **1** (12.8 μL , 0.1 mmol, 1.0 eq.), methyl 4-iodobenzoate (40.1 mg, 0.15 mmol, 1.5 eq.), AgOAc (25 mg, 0.15 mmol, 1.5 eq.) and 100 μL of stock solution containing Pd(OAc)₂ (0.1 M), S,O-ligand **L2** (0.1 M) and NBE **N2** (0.5 M). The tubes were placed in a pre-heated oil bath at 90 °C and stirred for the indicated time. The reaction tube was cooled in an ice bath and filtered through Celite® and rinsed with DCM. To the crude mixture CH₂Br₂ (7.08 μL , 0.1 mmol) was added as internal standard, the mixture was dissolved in CDCl₃ and ¹H NMR was measured.

Table 11. Kinetic profile of catalytic reaction – DCE.**Order of reagents via initial rate kinetics – HFIP**

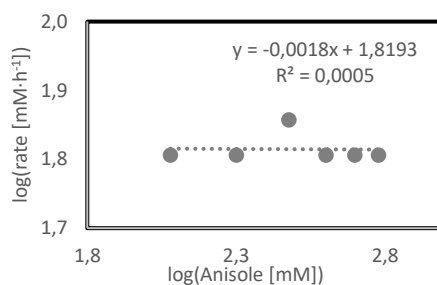
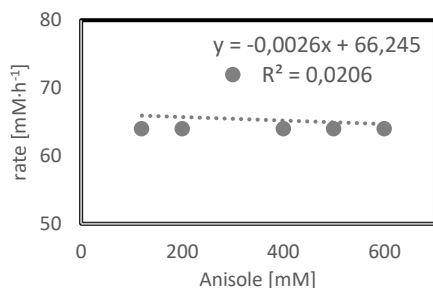
The reaction order of each reagent was determined using the initial rate method.^[22]

Five-seven pressure tubes containing a suitable stirring were equipped with 3-methylanisole **1b** (12.8 μL , 0.1 mmol, 1.0 eq.), methyl 4-iodobenzoate (40.1 mg, 0.15 mmol, 1.5 eq.), AgOAc (25 mg, 0.15 mmol, 1.5 eq.) and 100 μL of stock solution in HFIP containing Pd(OAc)₂ (0.05 M), S,O-ligand **L2** (0.05 M) and NBE **N2** (0.5 M) and 0.15 mL HFIP. The tubes were placed in a pre-heated oil bath at 90 °C and stirred for 30 min. The reaction tube was cooled in an ice bath, filtered through Celite® and rinsed with DCM. To the crude mixture CH₂Br₂ (7.08 μL , 0.1 mmol) was added as internal standard, the mixture was dissolved in CDCl₃ and ¹H NMR was measured.

The amounts of reagents were varied according to the tables. For the determination of the order of catalyst and NBE two separate stock solutions were made one only containing NBE **N2** and one containing Pd(OAc)₂/**L2**. In all cases, the total solvent amount was adjusted to 0.25 ml (0.4 M).

Table 12. Determination of reaction order of Anisole (0.15 mmol Ar-I, 0.05 mmol. NBE, 0.005 mmol Pd(OAc)₂/L1 and 0.15 mmol AgOAc – HFIP 0.4 M).

#	Anisole 1 [mmol]	Anisole 1 [mM]	log (Anisole 1 [mM])	3 [%]	3 [mmol]	3 [mM]	rate [mM·h ⁻¹]	log (rate [mM·h ⁻¹])
1	0,030	120	2,1	8	0,008	32	64	1,8
2	0,050	200	2,3	8	0,008	32	64	1,8
3	0,075	300	2,5	9	0,009	36	72	1,9
4	0,100	400	2,6	8	0,008	32	64	1,8
5	0,125	500	2,7	8	0,008	32	64	1,8
6	0,150	600	2,8	8	0,008	32	64	1,8

**Table 13.** Determination of reaction order of Ar-I (0.1 mmol Anisole, 0.05 mmol NBE, 0.005 mmol Pd(OAc)₂/L1 and 0.15 mmol AgOAc – HFIP 0.4 M).

#	Ar-I 2 [mmol]	Ar-I 2 [mM]	log (Ar-I 2 [mM])	3 [%]	3 [mmol]	3 [mM]	rate [mM·h ⁻¹]	log (rate [mM·h ⁻¹])
1	0,025	100	2,0	3	0,003	12	24	1,4
2	0,050	200	2,3	5	0,005	18	36	1,6
3	0,075	300	2,5	6	0,006	24	48	1,7
4	0,100	400	2,6	7	0,007	28	56	1,7
5	0,125	500	2,7	8	0,008	32	64	1,8
6	0,150	600	2,8	9	0,009	36	72	1,9
7	0,175	700	2,8	10	0,010	40	80	1,9

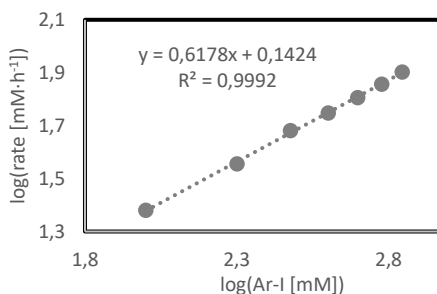
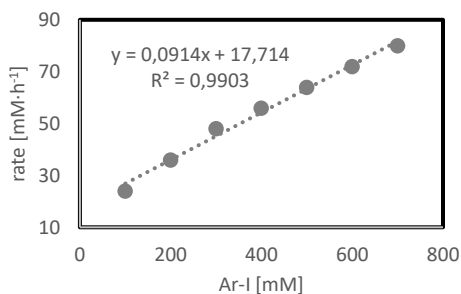
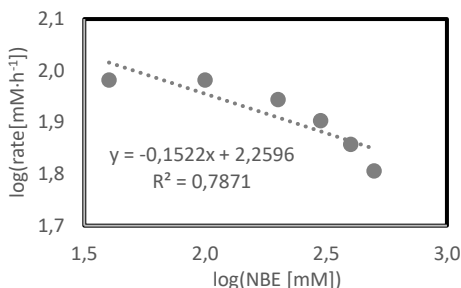
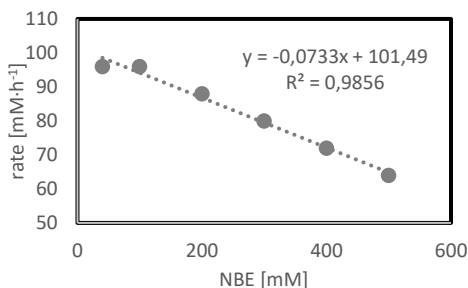


Table 14. Determination of reaction order of NBE (0.1 mmol Anisole, 0.15 mmol Ar-I, 0.005 mmol Pd(OAc)₂/L1 and 0.15 mmol AgOAc – HFIP 0.4 M).

#	NBE N1 [mmol]	NBE N1 [mM]	log (NBE N1 [mM])	3 [%]	3 [mmol]	3 [mM]	rate [mM·h ⁻¹]	log (rate [mM·h ⁻¹])
1	0,010	40	1,6	12	0,012	48,000	96	2,0
2	0,025	100	2,0	12	0,012	48,000	96	2,0
3	0,050	200	2,3	11	0,011	44,000	88	1,9
4	0,075	300	2,5	10	0,010	40,000	80	1,9
5	0,100	400	2,6	9	0,009	36,000	72	1,9
6	0,125	500	2,7	8	0,008	32,000	64	1,8

**Table 15.** Determination of reaction order of Pd(OAc)₂/L2 (0.1 mmol. Anisole, 0.15 mmol Ar-I, 0.05 mmol NBE and 0.15 mmol AgOAc – HFIP 0.4 M).

#	Pd/L1 [mmol]	Pd/L1 [mM]	log (Pd/L1 [mM])	3 [%]	3 [mmol]	3 [mM]	rate [mM·h ⁻¹]	log (rate [mM·h ⁻¹])
1	0,0010	4	0,6	1,00	0,001	4,000	8	0,9
2	0,0025	10	1,0	4,00	0,004	16,000	32	1,5
3	0,0050	20	1,3	9,00	0,009	36,000	72	1,9
4	0,0075	30	1,5	12,00	0,012	48,000	96	2,0
5	0,0100	40	1,6	16,00	0,016	64,000	128	2,1

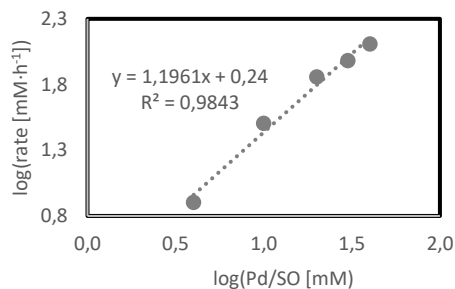
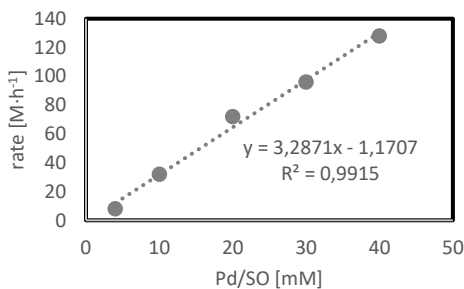
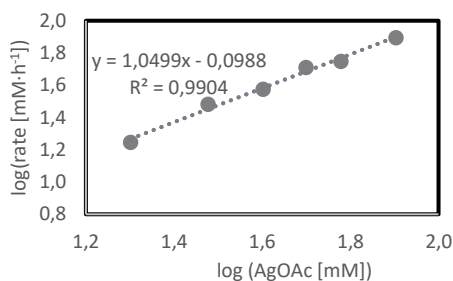
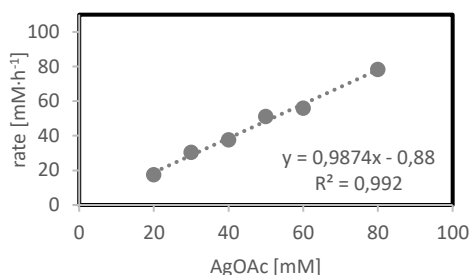


Table 16. Determination of reaction order of AgOAc (0.1 mmol Anisole, 0.15 mmol Ar-I, 0.005 mmol Pd(OAc)₂/L1, 0.05 mmol NBE – HFIP 0.4 M).

#	AgOAc [mmol]	AgOAc [mM]	log (AgOAc [mM])	3 [%]	3 [mmol]	3 [mM]	rate [mM·h ⁻¹]	log (rate [mM·h ⁻¹])
1	0,0050	20	1,3	2,20	0,002	8,8	18	1,2
2	0,0075	30	1,5	3,80	0,004	15,2	30	1,5
3	0,0100	40	1,6	4,70	0,005	18,8	38	1,6
4	0,0125	50	1,7	6,40	0,006	25,6	51	1,7
5	0,0150	60	1,8	7,00	0,007	28,0	56	1,7
6	0,0200	80	1,9	9,80	0,010	39,2	78	1,9

**Order of reagents via initial rate kinetics – DCE**

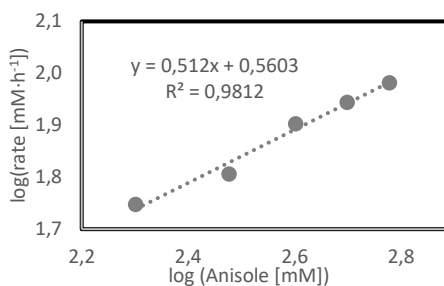
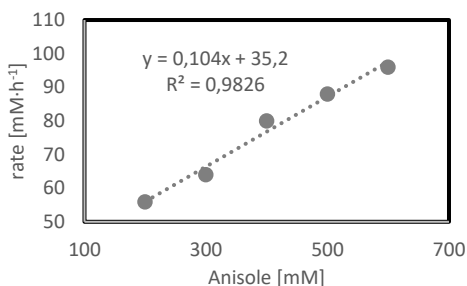
The reaction order of each reagent was determined using the initial rate method.^[22]

5-6 pressure tubes containing a suitable stirring were equipped with 3-methylanisole **1b** (12.8 μ L, 0.1 mmol, 1.0 eq.), methyl 4-iodobenzoate (40.1 mg, 0.15 mmol, 1.5 eq.), AgOAc (25 mg, 0.15 mmol, 1.5 eq.) and 100 μ L of stock solution in DCE containing Pd(OAc)₂ (0.1 M), S,O-ligand **L1** (0.1 M) and NBE **N1** (0.5 M) and 0.15 mL DCE. The tubes were placed in a pre-heated oil bath at 90 °C and stirred for 30 min. The reaction tube was cooled in an ice bath and filtered through Celite® and rinsed with DCM. To the crude mixture CH₂Br₂ (7.08 μ L, 0.1 mmol) was added as internal standard, the mixture was dissolved in CDCl₃ and ¹H NMR was measured.

The amounts of reagents were varied according to the tables. For the determination of the order of catalyst and NBE two separate stock solutions were made one only containing NBE **N1** and one containing Pd(OAc)₂/ **L1**. In all cases the total solvent amount was adjusted to 0.25 ml (0.4 M).

Table 17. Determination of reaction order of Anisole (0.15 mmol. Ar-I, 0.05 mmol NBE, 0.01 mmol Pd(OAc)₂/L1 and 0.15 mmol AgOAc – DCE 0.4 M).

#	Anisole 1 [mmol]	Anisole 1 [mM]	log (Anisole 1 [mM])	3 [%]	3 [mmol]	3 [mM]	rate [mM·h ⁻¹]	log (rate [mM·h ⁻¹])
1	0,050	200	2,3	7,00	0,007	28	56	1,7
2	0,075	300	2,5	8,00	0,008	32	64	1,8
3	0,100	400	2,6	10,00	0,010	40	80	1,9
4	0,125	500	2,7	11,00	0,011	44	88	1,9
5	0,150	600	2,8	12,00	0,012	48	96	2,0

**Table 18.** Determination of reaction order of Ar-I (0.1 mmol Anisole, 0.05 mmol NBE, 0.01 mmol Pd(OAc)₂/L1 and 0.15 mmol. AgOAc – DCE 0.4 M).

#	Ar-I 2 [mmol]	Ar-I 2 [mM]	log (Ar-I 2 [mM])	3 [%]	3 [mmol]	3 [mM]	rate [mM·h ⁻¹]	log (rate [mM·h ⁻¹])
1	0,050	200	2,3	6	0,006	24	48	1,7
2	0,075	300	2,5	8	0,008	32	64	1,8
3	0,100	400	2,6	10	0,010	40	80	1,9
4	0,125	500	2,7	11	0,011	44	88	1,9
5	0,150	600	2,8	12	0,012	48	96	2,0

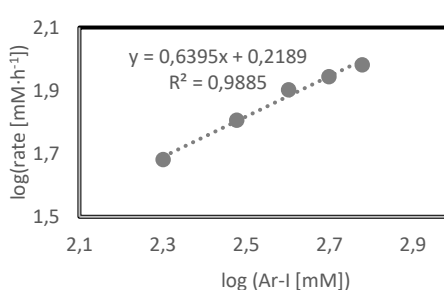
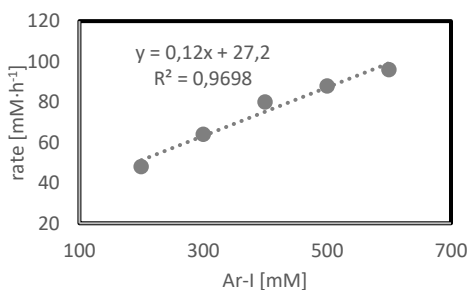
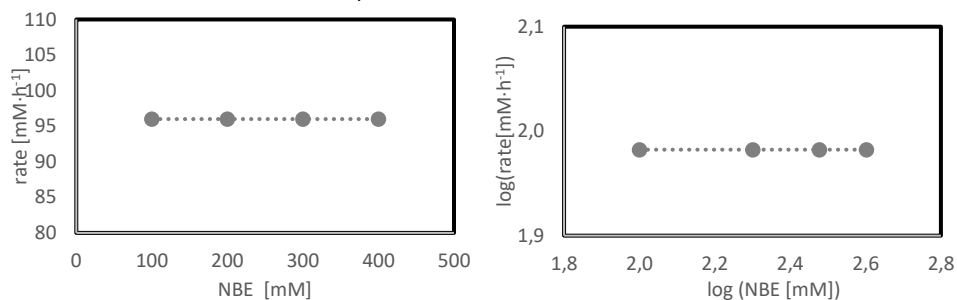


Table 19. Determination of reaction order of NBE (0.1 mmol. Anisole, 0.15 mmol. Ar-I, 0.01 mmol Pd(OAc)₂/L1 and 0.15 mmol AgOAc – DCE 0.4 M).

#	NBE N1 [mmol]	NBE N1 [mM]	log (NBE N1 [mM])	3 [%]	3 [mmol]	3 [mM]	rate [mM·h ⁻¹]	log (rate [mM·h ⁻¹])
1*	0,010	40	1,6	6	0,006	24	48	1,7
2	0,025	100	2,0	12	0,012	48	96	2,0
3	0,050	200	2,3	12	0,012	48	96	2,0
4	0,075	300	2,5	12	0,012	48	96	2,0
5	0,100	400	2,6	12	0,012	96	2,0	

*For the determination of the order entry 1 was excluded.

**Table 20.** Determination of reaction order of Pd(OAc)₂/L1 (0.1 mmol. Anisole, 0.15 mmol Ar-I, 0.05 mmol NBE and 0.15 mmol AgOAc – DCE 0.4 M).

#	Pd/L1 [mmol]	Pd/L1 [mM]	log (Pd/L1 [mM])	3 [%]	3 [mmol]	3 [mM]	rate [mM·h ⁻¹]	log (rate [mM·h ⁻¹])
1	0,0050	20	1,3	5,5	0,006	22	44	1,6
2	0,0075	30	1,5	7,5	0,008	30	60	1,8
3	0,0100	40	1,6	9,0	0,009	36	72	1,9
4	0,0125	50	1,7	11,0	0,011	44	88	1,9
5	0,0150	60	1,8	13,5	0,014	54	108	2,0

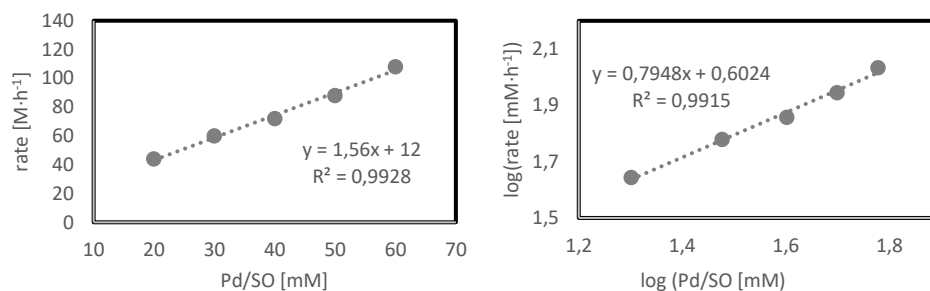
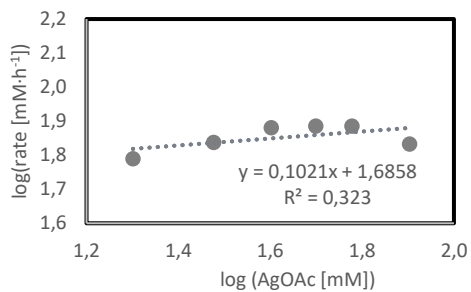
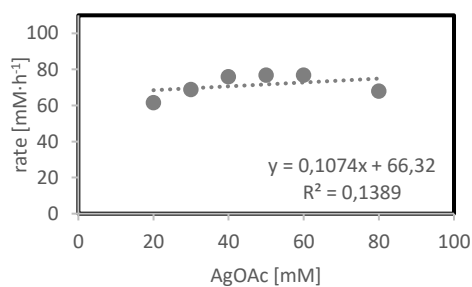


Table 21. Determination of reaction order of AgOAc (0.1 mmol Anisole, 0.15 mmol Ar-I, 0.01 mmol Pd(OAc)₂/L1, 0.05 mmol NBE – DCE 0.4 M).

#	AgOAc [mmol]	AgOAc [mM]	log (AgOAc [mM])	3 [%]	3 [mmol]	3 [mM]	rate [mM·h ⁻¹]	log (rate [mM·h ⁻¹])
1	0,0050	20	1,3	0,008	0,008	31	62	1,8
2	0,0075	30	1,5	0,009	0,009	34	69	1,8
3	0,0100	40	1,6	0,010	0,010	38	76	1,9
4	0,0125	50	1,7	0,010	0,010	38	77	1,9
5	0,0150	60	1,8	0,010	0,010	38	77	1,9
6	0,0200	80	1,9	0,009	0,009	34	68	1,8



Kinetic profile of stoichiometric reaction in HFIP

19 pressure tubes containing a suitable stirring were equipped with 3-methylanisole **1b** (6.36 μL , 0.05 mmol, 1.0 eq.), **N2** (7 μL , 0.05 mmol, 1.2 eq.), Pd(OAc)₂ (11.3 mg, 0.05 mmol, 1.0 eq.), S,O-ligand **L2** (14.3 mg, 0.05 mmol, 1.0 eq.), methyl 4-iodobenzoate (19.6 mg, 0.075 mmol, 1.5 eq.) and in 10 pressure tubes AgOAc (12.5 mg, 0.075 mmol, 1.5 eq.). 0.125 mL HFIP was added and the tubes were placed in a pre-heated oil bath at 90 °C and stirred for the indicated time. After cooling in an ice bath, the reaction was filtered through Celite® and rinsed with DCM. To the crude mixture CH₂Br₂ (3.54 μL , 0.05 mmol) was added as internal standard, the mixture was dissolved in CDCl₃ and ¹H NMR was measured.

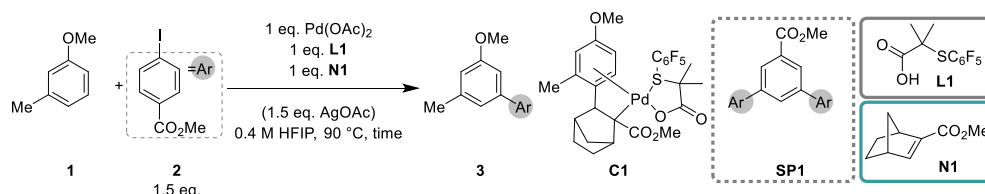


Table 22. Kinetic profile of stoichiometric reaction in HFIP with AgOAc.

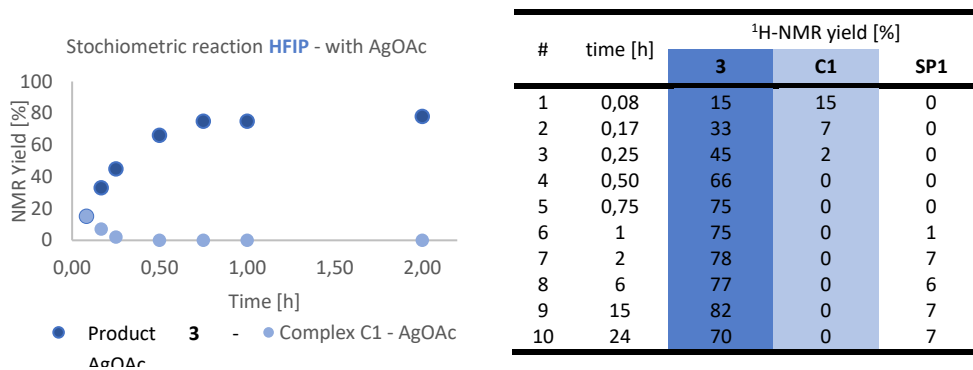
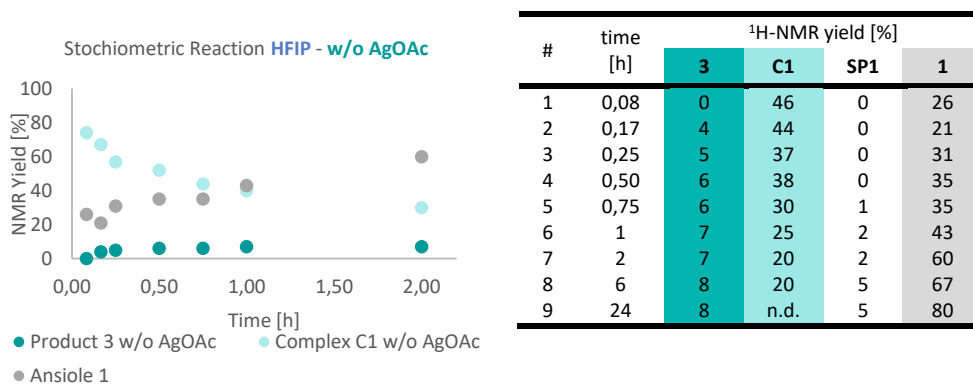
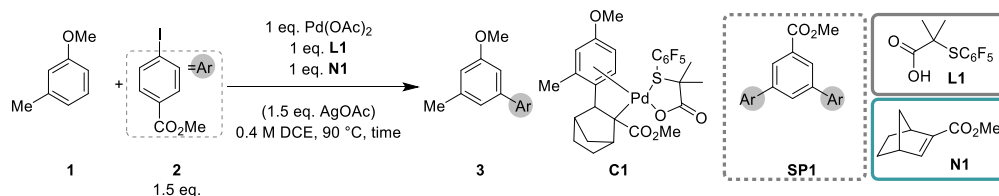
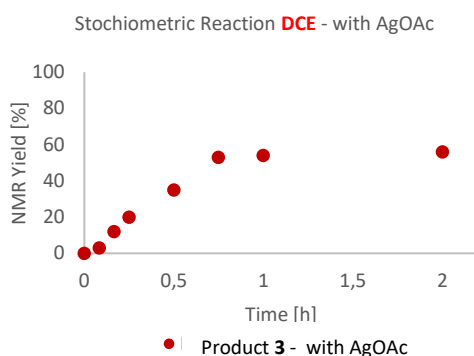


Table 23. Kinetic Profile of Stoichiometric Reaction in HFIP without AgOAc.

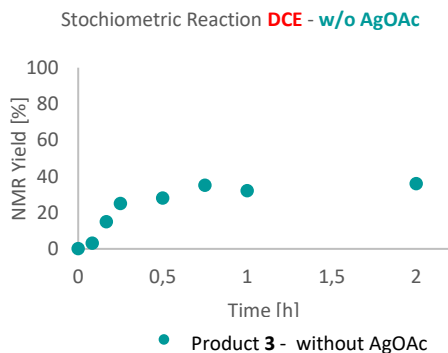


Kinetic profile of stoichiometric reaction in DCE with AgOAc

19 pressure tubes containing a suitable stirring were equipped with 3-methylanisole **1b** (6.36 μL , 0.05 mmol, 1.0 eq.), **N2** (7 μL , 0.05 mmol, 1.2 eq.), Pd(OAc)₂ (11.3 mg, 0.05 mmol, 1.0 eq.), S,O-ligand **L2** (14.3 mg, 0.05 mmol, 1.0 eq.), methyl 4-iodobenzoate (19.6 mg, 0.075 mmol, 1.5 eq.) and in 9 pressure tubes AgOAc (12.5 mg, 0.075 mmol, 1.5 eq.). 0.125 mL DCE was added and the tubes were placed in a pre-heated oil bath at 90 °C and stirred for the indicated time. After cooling in an ice bath, the reaction was filtered through Celite® and rinsed with DCM. To the crude mixture CH₂Br₂ (3.54 μL , 0.05 mmol) was added as internal standard, the mixture was dissolved in CDCl₃ and ¹H NMR was measured.

**Table 24.** Kinetic profile of stoichiometric reaction in DCE with AgOAc.

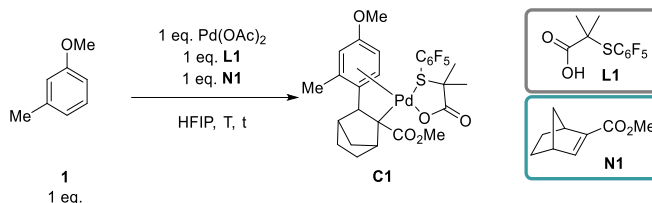
#	time [h]	¹ H-NMR yield [%]		
		3	C1	SP1
1	0,08	0	0	0
2	0,17	4	0	0
3	0,25	21	0	0
4	0,50	22	0	0
5	0,75	44	0	0
6	1	53	0	1
7	2	54	0	9
8	6	56	0	10
9	24	52	0	10

Table 25. Kinetic profile of stoichiometric reaction in DCE without AgOAc.

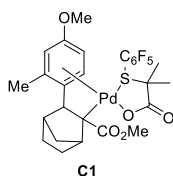
#	time [h]	¹ H-NMR yield [%]		
		3	C1	SP1
1	0,08	3	0	0
2	0,17	15	0	0
3	0,25	25	0	1
4	0,50	28	0	4
5	0,75	35	0	6
6	1	32	0	6
7	2	36	0	10
8	6	40	0	13
9	15	41	0	15
10	24	40	0	18

Synthesis of complex C1

The optimization of the synthesis of complex **C1** was performed by adding 3-methylanisole (12.8 μL , 0.1 mmol, 1.0 eq), Pd(OAc)₂ (22.8 mg, 0.1 mmol, 1.0 eq), **N1** (15.2 mg, 0.1 mmol, 1.0 eq), **L1** (28.6 mg, 0.1 mmol, 1.0 eq) and HFIP (0.25 mL, 0.4 M) in a pressure tube and the mixture stirred at the indicated temperature and for the indicated time. After cooling to room temperature, the reaction was filtrated through Celite® and rinsed with DCM. The solvent was removed under reduced pressure and to the crude mixture CH₂Br₂ (7.08 μL , 0.1 mmol) was added as an internal standard, the mixture was dissolved in CDCl₃ and ¹H NMR was measured.

Table 26. Optimization of conditions to obtain complex **C1**.

#	Solvent 0.4 M	Temp. [°C]	Time [h]	¹ H-NMR yield [%] C1a
1	HFIP	90	2	70
2	HFIP	90	4	40
3	HFIP	60	0.25	76
4	HFIP	60	0.5	85
5	HFIP	60	1	70
6	HFIP	60	2	70

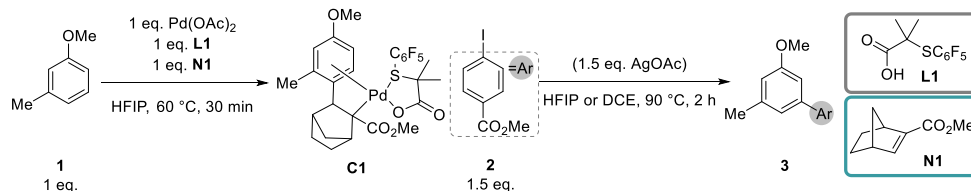
Complex C1

Complex **C1** was synthesized by adding 3-methylanisole (12.8 μL , 0.1 mmol, 1.0 eq), Pd(OAc)₂ (22.8 mg, 0.1 mmol, 1.0 eq), **N1** (15.2 mg, 0.1 mmol, 1.0 eq.), **L1** (28.6 mg, 0.1 mmol, 1.0 eq) and HFIP (0.25 mL, 0.4 M) in a pressure tube and the mixture stirred for 30 min at 60 °C. After cooling to room temperature, the reaction was filtrated through Celite® and rinsed with DCM. The solvent was evaporated under reduced pressure. To the crude mixture CH₂Br₂ (7.08 μL , 0.1 mmol) was added as internal standard, the mixture was dissolved in CDCl₃ and ¹H NMR was measured, providing the complex **C1** in 85% ¹H NMR yield. Attempts

to purify the crude by column chromatography on silica gel using Cy / EtOAc / MeOH (1:1:0-9:1 v/v) or by crystallization were unsuccessful as new impurities appeared. [Note: we assume, that complex **C1** is less stable due to steric hinderance in comparison to complex **C1a**, which might explain the difficulties to isolate it purely]. Due to the clear crude NMR, we decided to give proton signals of the complex in the crude and compare the signals with **C1a**. Two Rotamers in a ratio of a:b = 2:1 are observed and about 10% of 3-methylanisole **1a** remains in the crude NMR. ¹H NMR (400 MHz, CDCl₃) δ 8.22 (d, J = 8.9 Hz, 1H_b), 7.97 (d, J = 7.7 Hz, 1H_a), 6.98 – 6.84 (m, 2H_{a+b}), 4.00 (s, 3H_a), 3.85 (s, 3H_b), 3.78 (s, 1H_{a+b}), 3.40 (s, 3H_a), 3.31 (s, 3H_b), 3.13 (d, J = 10.4 Hz, 1H_b), 3.03 (d, J = 10.1 Hz, 1H_a), 2.83 (s, 1H_{a+b}), 2.38 (s, 3H_{a+b}), 2.19 (s, 1H_{a+b}), 1.74 – 1.02 (m, 11H_{a+b}).

Reaction of complex C1 with Ar-I 2

5 pressure tubes containing a suitable stirring were equipped with 2-methylanisole **1b** (12.8 μ L, 0.1 mmol, 1.0 eq.), Pd(OAc)₂ (22.8 mg, 0.1 mmol, 1.0 eq.), S,O-ligand **L2** (28.6 mg, 0.1 mmol, 1.0 eq.) and NBE **N2** (15.2 mg, 0.1 mmol, 1.0 eq.). HFIP (0.25 mL, 0.4 M) was added and the tubes were placed in a pre-heated oil bath at 60 °C and stirred for 30 min. After cooling in an ice bath, the reaction was filtered through Celite® and rinsed with DCM. To one of the crude mixtures CH₂Br₂ (7.08 μ L, 0.1 mmol) was added as internal standard, the mixture was dissolved in CDCl₃ and ¹H NMR was measured (Table **SX** - entry 1). To the other four crude mixtures methyl 4-iodobenzoate (40.1 mg, 0.15 mmol, 1.5 eq.) and to only two of these four crude mixtures AgOAc (25 mg, 0.15 mmol, 1.5 eq.) (Table **SX** - entry 2+4) was added. HFIP or DCE (0.25 mL, 0.4 M) were added and the reactions were placed in a pre-heated oil bath at 90 °C and stirred for the 2 h. After cooling to room temperature, the reaction was filtered through Celite® and rinsed with DCM. To the crude mixtures CH₂Br₂ (7.08 μ L, 0.1 mmol) was added as internal standard, the mixture was dissolved in CDCl₃ and ¹H NMR was measured.

Table 27. Reaction of Complex **C1** with Ar-I **2**.

#	Solvent 0.4 M	AgOAc [eq.]	¹ H-NMR yield [%]	
			3a	C1
1	HFIP	-	n.a.	85
2	HFIP	1.5 eq.	75	-
3	HFIP	-	10	41
4	DCE	1.5 eq.	70	-
5	DCE	-	61	10

NMR Experiments of complex C1 and C1a

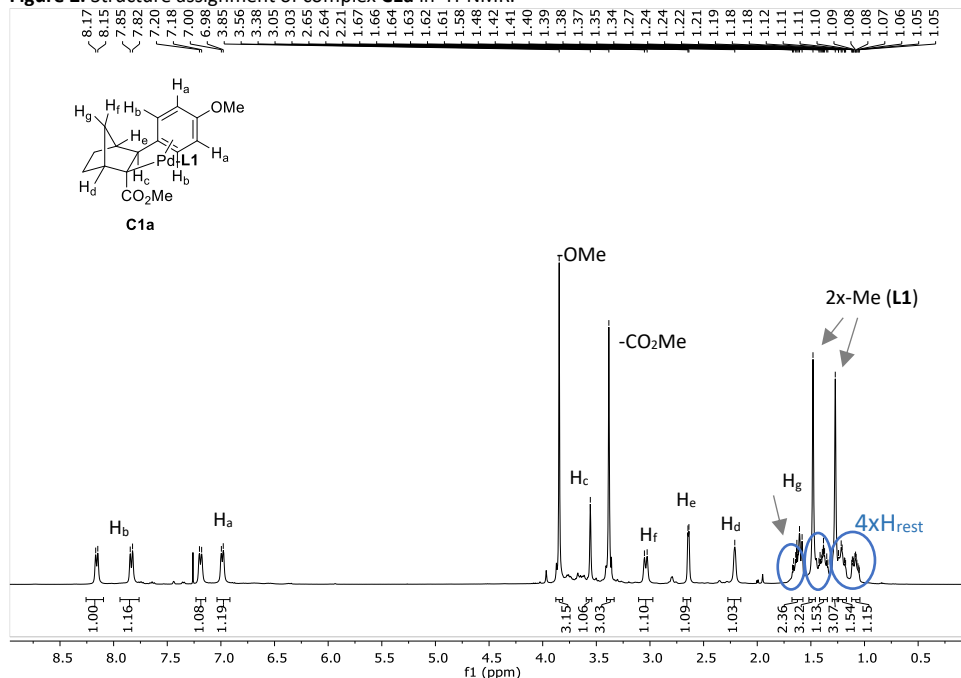
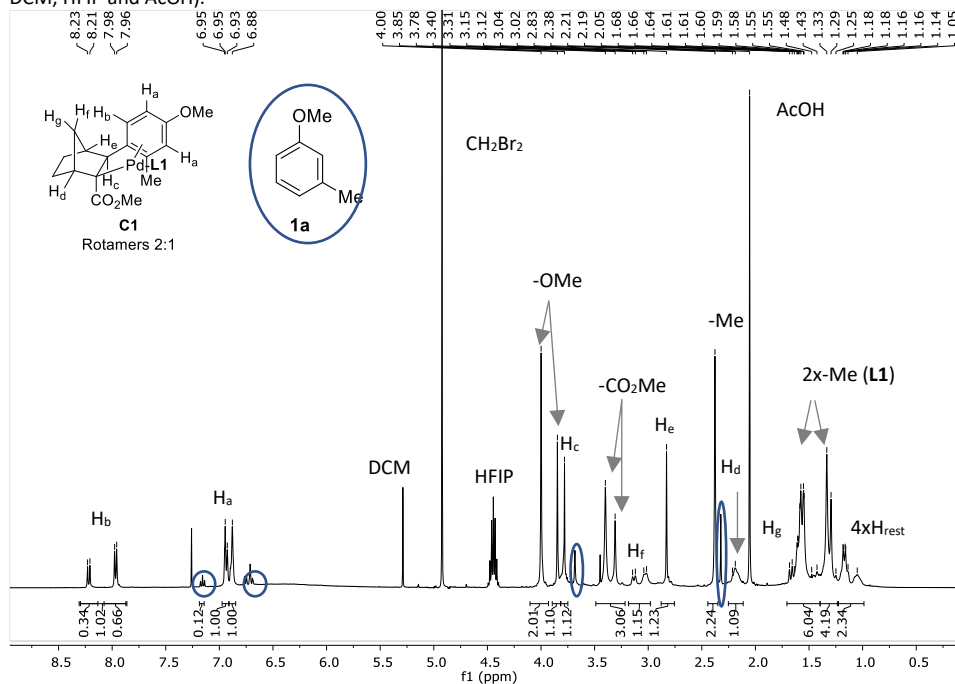
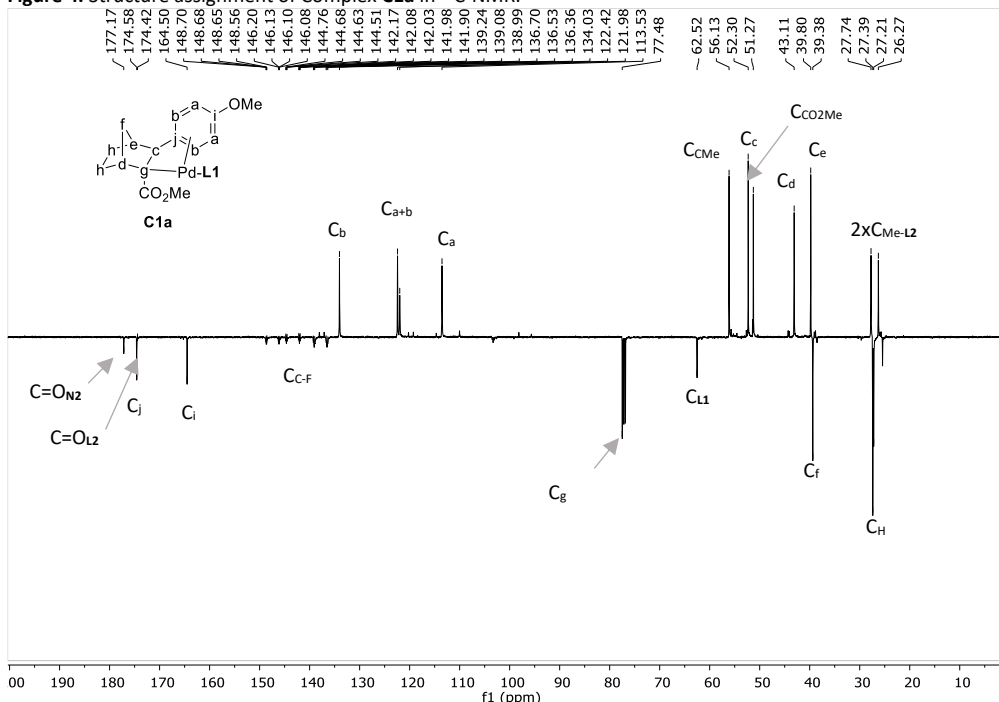
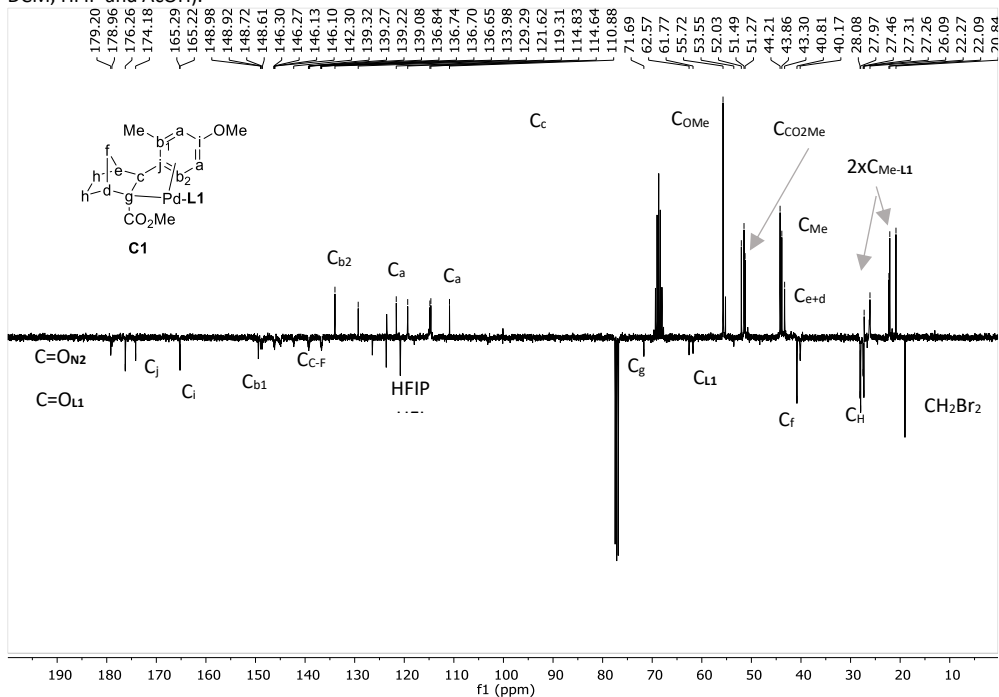
Figure 2. Structure assignment of complex C1a in $^1\text{H-NMR}$.Figure 3. Structure assignment of complex C1 in $^1\text{H-NMR}$ (Crude NMR – contains 10% 1a 2-Methylanisole, CH₂Br₂, DCM, HFIP and AcOH).

Figure 4. Structure assignment of Complex **C1a** in ^{13}C -NMR.**Figure 5.** Structure assignment of Complex **C1** in ^{13}C -NMR (Crude NMR – contains 10% **1a** 2-Methylanisole, CH₂Br₂, DCM, HFIP and AcOH).

6.5 References and notes

- [1] For selected reviews of directing group assisted C–H functionalization: a) M. O. Tischler, M. B. Tóth, Z. Novák, *Chem. Rev.* **2017**, *17*, 184–199; b) C. Sambiagio, D. Schönbauer, R. Blicek, T. Dao-Huy, G. Pototschnig, P. Schaaf, T. Wiesinger, M. F. Zia, J. Wencel-Delord, T. Besset, B. U. W. Maes, M. Schnürch, *Chem. Soc. Rev.* **2018**, *47*, 6603–6743; c) K. Murali, L. A. Machado, R. L. Carvalho, L. F. Pedrosa, R. Mukherjee, E. N. Da Silva Júnior, D. Maiti, *Chem. Eur. J.* **2021**, *27*, 12453–12508; For selected reviews of non-directed C–H functionalization: d) N. Kuhl, M. N. Hopkinson, J. Wencel-Delord, F. Glorius, *Angew. Chem. Int. Ed.* **2012**, *51*, 10236–10254; e) A. Dey, S. Maity, D. Maiti, *Chem. Comm.* **2016**, *52*, 12398–12414; f) P. Wedi, M. van Gemmeren, *Angew. Chem. Int. Ed.* **2018**, *57*, 13016–13027; g) S. Kancherla, K. B. Jorgensen, M. Á. Fernández-Ibáñez, *Synthesis* **2019**, *51*, 643–663.
- [2] For reviews of silver in C–H functionalization: a) J. M. Weibel, A. Blanc, P. Pale, *Chem. Rev.* **2008**, *108*, 3149–3173; b) O. Daugulis, H. Do, D. Shabashov, *Acc. Chem. Res.* **2009**, *42*, 1074–1086; c) K. L. Bay, Y. F. Yang, K. N. Houk, *J. Organomet. Chem.* **2018**, *864*, 19–25; d) Á. L. Mudarra, S. Martínez De Salinas, M. H. Pérez-Temprano, *Org. Biomol. Chem.* **2019**, *17*, 1655–1667; e) T. Bhattacharya, S. Dutta, D. Maiti, *ACS Catal.* **2021**, *11*, 9702–9714; f) A. Mondal, M. van Gemmeren, *Angew. Chem. Int. Ed.* **2022**, e202210825.
- [3] For selected examples of silver as a terminal oxidant: a) P. Wang, P. Verma, G. Xia, J. Shi, J. X. Qiao, S. Tao, P. T. W. Cheng, M. A. Poss, M. E. Farmer, K. S. Yeung, J. Q. Yu, *Nature* **2017**, *551*, 489–493; b) H. Chen, P. Wedi, T. Meyer, G. Tavakoli, M. van Gemmeren, *Angew. Chem. Int. Ed.* **2018**, *57*, 2497–2501; c) B. Yin, M. Fu, L. Wang, J. Liu, Q. Zhu, *Chem. Comm.* **2020**, *56*, 3293–3296.
- [4] For selected examples of silver catalyzed C–H activation in palladium catalysis: a) D. Whitaker, J. Burés, I. Larrosa, *J. Am. Chem. Soc.* **2016**, *138*, 8384–8387; b) S. Y. Lee, J. F. Hartwig, *J. Am. Chem. Soc.* **2016**, *138*, 15278–15284; c) M. D. Lotz, N. M. Camasso, A. J. Canty, M. S. Sanford, *Organometallics* **2017**, *36*, 165–171; d) C. Colletto, A. Panigrahi, J. Fernández-Casado, I. Larrosa, *J. Am. Chem. Soc.* **2018**, *140*, 9638–9643; e) A. Tlahuext-Aca, S. Y. Lee, S. Sakamoto, J. F. Hartwig, *ACS Catal.* **2021**, *11*, 1430–1434; f) G. Athavan, T. F. N. Tanner, A. C. Whitwood, I. J. S. Fairlamb, R. N. Perutz, *Organometallics* **2022**, *41*, 3175–3184; g) J. Yao, J. Bai, X. Kang, M. Zhu, Y. Guo, X. Wang, *Nanoscale* **2023**, *15*, 3560–3565.
- [5] For selected examples of Pd/Ag bi- or multimetallic catalyzed C–H activation: a) S. Lee, H. Lee, K. L. Tan, *J. Am. Chem. Soc.* **2013**, *135*, 18778–18781; b) Y. F. Yang, G. J. Cheng, P. Liu, D. Leow, T. Y. Sun, P. Chen, X. Zhang, J. Q. Yu, Y. D. Wu, K. N. Houk, *J. Am. Chem. Soc.* **2014**, *136*, 344–355; c) M. Anand, R. B. Sunoj, H. F. Schaefer, *J. Am. Chem. Soc.* **2014**, *136*, 5535–5538; d) M. Anand, R. B. Sunoj, H. F. Schaefer, *ACS Catal.* **2016**, *6*, 696–708; e) L. Zhang, C. Zhao, Y. Liu, J. Xu, X. Xu, Z. Jin, *Angew. Chem. Int. Ed.* **2017**, *56*, 12245–12249; f) L. Fang, T. G. Saint-Denis, B. L. H. Taylor, S. Ahlquist, K. Hong, S. Liu, L. Han, K. N. Houk, J. Q. Yu, *J. Am. Chem. Soc.* **2017**, *139*, 10702–10714; g) W. Feng, T. Wang, D. Liu, X. Wang, Y. Dang, *ACS Catal.* **2019**, *9*, 6672–6680; h) A. Panigrahi, D. Whitaker, I. J. Vitorica-Yrezabal, I. Larrosa, *ACS Catal.* **2020**, *10*, 2100–2107.
- [6] For selected examples of silver as a halide scavenger in directed C–H functionalization: a) O. Daugulis, V. G. Zaitsev, *Angew. Chem. Int. Ed.* **2005**, *44*, 4046–4048; b) D. Shabashov, O. Daugulis, *Org. Lett.* **2005**, *7*, 3657–3659; c) V. G. Zaitsev, D. Shabashov, O. Daugulis, *J. Am. Chem. Soc.* **2005**, *127*, 13154–13155; d) H. A. Chiong, Q. N. Pham, O. Daugulis, *J. Am. Chem. Soc.* **2007**, *129*, 9879–9884; e) V. S. Thirunavukkarasu, K. Parthasarathy, C. H. Cheng, *Angew. Chem. Int. Ed.* **2008**, *47*, 9462–9465; f) D. Shabashov, J. R. M. Maldonado, O. Daugulis, *J. Am. Chem. Soc.* **2008**, *73*, 7818–7821; g) F. Yang, Y. Wu, Z. Zhu, J. Zhang, Y. Li, *Tetrahedron* **2008**, *64*, 6782–6787; h) N. Rodríguez, J. A. Romero-Revilla, M. Á. Fernández-Ibáñez, J. C. Carretero, *Chem. Sci.* **2013**, *4*, 175–179; i) C. Zhu, Y. Zhang, J. Kan, H. Zhao, W. Su, *Org. Lett.* **2015**, *17*, 3418–3421; j) N. Dastbaravardeh, T. Toba, M. E. Farmer, J. Q. Yu, *J. Am. Chem. Soc.* **2015**, *137*, 9877–9884; k) Y. Zhu, X. Chen, C. Yuan, G. Li, J. Zhang, Y. Zhao, *Nat. Commun.* **2017**, *8*, 14904; l) T. Sheng, L. Hu, X. Cai, J. Yu, *Science* **2023**, *644*, 639–644.
- [7] For selected examples of silver as a halide scavenger in non-directed C–H functionalization: a) C. Qin, W. Lu, C. O. Ag, R. Bellina, R. C. O. Chem, *J. Org. Chem.* **2008**, *73*, 7424–7427; b) P. Ricci, K. Krämer, I. Larrosa, *J. Am. Chem. Soc.* **2014**, *136*, 18082–18086; c) R. Long, X. Yan, Z. Wu, Z. Li, H. Xiang, X. Zhou, *Org. Biomol. Chem.* **2015**, *13*, 3571–3574.
- [8] For selected examples of silver as a halide scavenger in C–H activation initiated Pd/NBE catalysis: a) X. C. Wang, W. Gong, L. Z. Fang, R. Y. Zhu, S. Li, K. M. Engle, J. Q. Yu, *Nature* **2015**, *519*, 334–338; b) G. C. Li, P. Wang, M. E. Farmer, J. Q. Yu, *Angew. Chemie - Int. Ed.* **2017**, *56*, 6874–6877; c) P. Wang, M. E. Farmer, X. Huo, P. Jain, P. X. Shen, M. Ishoey, J. E. Bradner, S. R. Wisniewski, M. D. Eastgate, J. Q. Yu, *J. Am. Chem. Soc.* **2016**, *138*, 9269–9276; d) Q. Li, E. M. Ferreira, *Chem. Eur. J.* **2017**, *23*, 11519–11523; e) J. Liu, Q. Ding, W. Fang, W. Wu, Y. Zhang, Y. Peng, *J. Org. Chem.* **2018**, *83*, 13211–13216; f) L. Y. Liu, J. X. Qiao, K. S. Yeung, W.

- R. Ewing, J. Q. Yu, *J. Am. Chem. Soc.* **2019**, *141*, 14870–14877; g) L. Y. Liu, J. X. Qiao, K. S. Yeung, W. R. Ewing, J. Q. Yu, *Angew. Chem. Int. Ed.* **2020**, *59*, 13831–13835; *Angew. Chem.* **2020**, *132*, 13935–13939; h) L. Y. Liu, J. X. Qiao, W. R. Ewing, K. S. Yeung, J. Q. Yu, *Isr. J. Chem.* **2020**, *60*, 416–418.
- [9] For selected examples with evidence that iodide abstraction takes place before reductive elimination: a) W. G. Whitehurst, J. H. Blackwell, G. N. Hermann, M. J. Gaunt, *Angew. Chem. Int. Ed.* **2019**, *58*, 9054–9059; b) L. J. Xiao, K. Hong, F. Luo, L. Hu, W. R. Ewing, K. S. Yeung, J. Q. Yu, *Angew. Chem. Int. Ed.* **2020**, *59*, 9594–9600; c) X. Ma, X. Zhao, R. Zhu, D. Zhang, *J. Org. Chem.* **2020**, *85*, 5995–6007.
- [10] a) Z. Dong, J. Wang, G. Dong, *J. Am. Chem. Soc.* **2015**, *137*, 5887–5890; b) R. Li, Y. Zhou, X. Xu, G. Dong, *J. Am. Chem. Soc.* **2019**, *141*, 18958–18963; c) R. Li, G. Dong, *Angew. Chem. Int. Ed.* **2021**, *60*, 26184–26191.
- [11] J. Wu, N. Kaplaneris, S. Ni, F. Kaltenhäuser, L. Ackermann, *Chem. Sci.* **2020**, *11*, 6521–6526.
- [12] a) A. Kubota, M. H. Emmert, M. S. Sanford, *Org. Lett.* **2012**, *14*, 1760–1763; b) X. Cong, H. Tang, C. Wu, X. Zeng, *Organometallics* **2013**, *32*, 6565–6575; c) K. Naksomboon, C. Valderas, M. Gómez-Martínez, Y. Álvarez-Casao, M. Á. Fernández-Ibáñez, *ACS Catal.* **2017**, *7*, 6342–6346; d) K. Naksomboon, J. Poater, F. M. Bickelhaupt, M. Á. Fernández-Ibáñez, *J. Am. Chem. Soc.* **2019**, *141*, 6719–6725; e) W. L. Jia, N. Westerveld, K. M. Wong, T. Morsch, M. Hakkenes, K. Naksomboon, M. Á. Fernández-Ibáñez, *Org. Lett.* **2019**, *21*, 9339–9342; f) V. Sukowski, W. Jia, R. Diest, M. Borselen, M. Á. Fernández-Ibáñez, *Eur. J. Org. Chem.* **2021**, 4132–4135; g) H. T. Kim, E. Kang, M. Kim, J. M. Joo, *Org. Lett.* **2021**, *23*, 3657–3662.
- [13] S. Panja, S. Ahsan, T. Pal, S. Kolb, W. Ali, S. Sharma, C. Das, J. Grover, A. Dutta, D. B. Werz, A. Paul, D. Maiti, *Chem. Sci.* **2022**, *13*, 9432–9439.
- [14] A. Saha, S. Guin, W. Ali, T. Bhattacharya, S. Sasmal, N. Goswami, G. Prakash, S. K. Sinha, H. B. Chandrashekar, S. Panda, S. S. Anjana, D. Maiti, *J. Am. Chem. Soc.* **2022**, *144*, 1929–1940.
- [15] For selected examples of Pd-catalyzed C–H arylation using aryl halides without the addition of silver salts: a) D. Shabashov, O. Daugulis, *J. Am. Chem. Soc.* **2010**, *132*, 3965–3972; b) Y. Mengchun, J. F. Edmunds, Andrew, J. A. Morris, D. Sale, Y. Zhanga, J.-Q. Yu, *Chem. Sci.* **2013**, *4*, 2374–2379; c) Q. Zhang, X. S. Yin, S. Zhao, S. L. Fang, B. F. Shi, *Chem. Comm.* **2014**, *50*, 8353–8355; d) Y. Wei, H. Tang, X. Cong, B. Rao, C. Wu, X. Zeng, *Org. Lett.* **2014**, *16*, 2248–2251; e) Q. Gou, G. Liu, L. Zhou, S. Chen, J. Qin, *Eur. J. Org. Chem.* **2017**, *42*, 6314–6318; f) S. K. Zhang, X. Y. Yang, X. M. Zhao, P. X. Li, J. L. Niu, M. P. Song, *Organometallics* **2015**, *34*, 4331–4339; g) S. Das, G. Bairy, R. Jana, *Org. Lett.* **2018**, *20*, 2667–2671; h) C. Arroniz, J. G. Denis, A. Ironmonger, G. Rassias, I. Larrosa, *Chem. Sci.* **2014**, *5*, 3509–3514; i) P. Wang, G. C. Li, P. Jain, M. E. Farmer, J. He, P. X. Shen, J. Q. Yu, *J. Am. Chem. Soc.* **2016**, *138*, 9269–9269; [Note: all reaction besides h) and i) are directing group assisted C(sp³)-H arylations.]
- [16] V. Sukowski, M. van Borselen, S. Mathew, M. Á. Fernández-Ibáñez, *Angew. Chem. Int. Ed.* **2022**, *134*, e202201750.
- [17] a) J. Wencel-Delord, F. Colobert, *Org. Chem. Front.* **2016**, *3*, 394–400; b) S. K. Sinha, T. Bhattacharya, D. Maiti, *React. Chem. Eng.* **2019**, *4*, 244–253; c) Ref V. Pozhydaiev, M. Power, V. Gandon, J. Moran, D. Leboeuf *Chem. Commun.*, **2020**, *56*, 11548–11556; d) T. Bhattacharya, A. Ghosh, D. Maiti, *Chem. Sci.* **2021**, *12*, 3857–3870.
- [18] Based on computational studies, a Pd/Ag binuclear catalyst has been proposed for the C–H activation step, see: X. Xu, K. Chen, *Org. Biomol. Chem.* **2020**, *18*, 5857–5866.
- [19] Note: Computational studies conducted by Zhang's group on similar reaction employing Pd/quinoxaline-based ligand/norbornene cooperative catalysis proposed that halide abstraction occurs prior to reductive elimination to lower the transition state energy: X. Ma, X. Zhao, R. Zhu, D. Zhang, *J. Org. Chem.* **2020**, *85*, 5995–6007.
- [20] S. J. Yun, J. Kim, E. Kang, H. Jung, H. T. Kim, M. Kim, J. M. Joo *ACS Catal.* **2023**, *13*, 4042–4052.
- [21] W. Ishiga, M. Ohta, T. Kodama, M. Tobisu *Org. Lett.* **2021**, *23*, 6714–6714.
- [22] J. H. Espenson, *Chemical kinetics and reaction mechanisms* (2nd ed.). McGraw Hill: **1987**.